2012

Injection-locked Semiconductor Lasers For Realization Of Novel Rf Photonics Components

Nazanin Hoghooghi
University of Central Florida

INJECTION-LOCKED SEMICONDUCTOR LASERS FOR REALIZATION OF NOVEL RF PHOTONICS COMPONENTS

by

NAZANIN HOGHOOGHI
B.S. Iran University of Science and Technology, 2005
M.S. Rose-Hulman Institute of Technology, 2007

A dissertation submitted in partial fulfillment of the requirements
for the degree of Doctor of Philosophy
in CREOL, The College of Optics and Photonics
at the University of Central Florida
Orlando, Florida

Summer Term
2012

Major Professor: Peter J. Delfyett, Jr.

ABSTRACT

This dissertation details the work has been done on a novel resonant cavity linear interferometric modulator and a direct phase detector with channel filtering capability using injection-locked semiconductor lasers for applications in RF photonics. First, examples of optical systems whose performance can be greatly enhanced by using a linear intensity modulator are presented and existing linearized modulator designs are reviewed. The novel linear interferometric optical intensity modulator based on an injection-locked laser as an arcsine phase modulator is introduced and followed by numerical simulations of the phase and amplitude response of an injection-locked semiconductor laser. The numerical model is then extended to study the effects of the injection ratio, nonlinear cavity response, depth of phase and amplitude modulation on the spur-free dynamic range of a semiconductor resonant cavity linear modulator. Experimental results of the performance of the linear modulator implemented with a multi-mode Fabry-Perot semiconductor laser as the resonant cavity are shown and compared with the theoretical model. The modulator performance using a vertical cavity surface emitting laser as the resonant cavity is investigated as well. Very low V_π in the order of 1 mV, multi-gigahertz bandwidth (-10 dB bandwidth of 5 GHz) and a spur-free dynamic range of 120 dB.Hz$^{2/3}$ were measured directly after the modulator. The performance of the modulator in an analog link is experimentally investigated and the results show no degradation of the modulator linearity after a 1 km of SMF.

The focus of the work then shifts to applications of an injection-locked semiconductor laser as a direct phase detector and channel filter. This phase detection technique does not

require a local oscillator. Experimental results showing the detection and channel filtering capability of an injection-locked semiconductor diode laser in a three channel system are shown. The detected electrical signal has a signal-to-noise ratio better than 60 dB/Hz.

In chapter 4, the phase noise added by an injection-locked vertical cavity surface emitting laser is studied using a self-heterodyne technique. The results show the dependency of the added phase noise on the injection ratio and detuning frequency.

The final chapter outlines the future works on the linear interferometric intensity modulator including integration of the modulator on a semiconductor chip and the design of the modulator for input pulsed light.

To my family

ACKNOWLEDGMENTS

I would like to thank past and present members of Ultrafast Photonics group for all their continuous supports. They are Prof. Peter Delfyett, Dr. Sarper Ozharar, Dr. Frank Quinlan, Dr. Ji-Myoung Kim, Dr. Ibrahim Ozdur, Dr. Dimitrios Mandridis, Mohammad Umar Piracha, Charles Williams, Sharad Bhooplapur, Abhijeet Ardey, Dat Nguyen, Josue Davila-Rodriguez, Marcus Bagnell, Edris Sarailou, Anthony Klee, and Kristina Bagnell. I would particularly like to emphasize the importance of Prof. Peter Delfyett, Dr. Ibrahim Ozdur and Josue Davila-Rodriguez without whom none of what follows would have been possible.

TABLE OF CONTENTS

LIST OF FIGURES

LIST OF TABLES

CHAPTER 1: INTRODUCTION

1.1 Injection locking of lasers

Injection locking of oscillators has been an area of interest for centuries. In 1865, Huygens first discovered the synchronization between two clocks on the wall even with different initial conditions [1]. The phenomenon did not begin to be understood until the development of nonlinear dynamics by Poincare, and Van der Pol who were the first to study the forced oscillation in detail. Alder [2] later demonstrated that this frequency locking synchronization between oscillators can also apply to electronic circuits and opened up a new era in communication.

Injection locking is the process of locking the frequency of a laser called slave laser, to another typically more stable laser called master laser, as illustrated in Figure 1.1. In this figure, ω_1 and ω_0 are the free running angular frequencies of the master and slave lasers, respectively. Injection locking occurs by coupling the light from the master laser into the slave laser cavity via a suitable coupling method. The power of the injected signal typically is much lower than the slave laser free running output power. If the frequency of the injection seed is within a frequency range called locking range, the frequency of slave laser will be locked to the frequency of the injected seed [3].

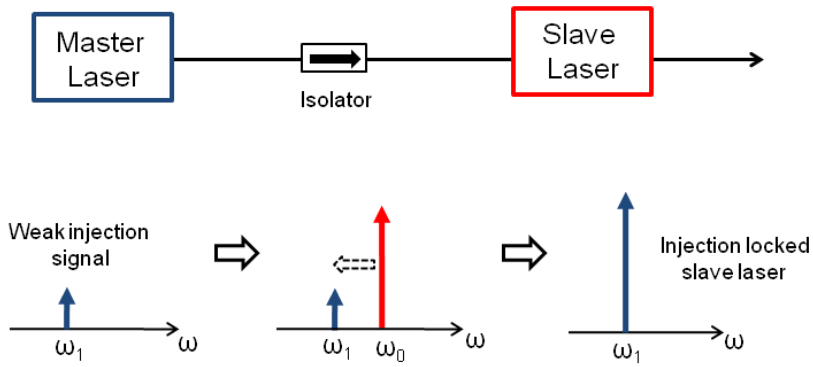

Figure 1.1. Injection locking of two lasers.

Depending on the frequency detuning and the injection power, the injection-locked laser can be stably locked, unstably locked or exhibit chaotic behavior. In the stable locking regime, injection locking improves the performance of the slave laser. Figure 1.2 shows the behavior of the slave laser for two cases: the injection seed is outside the locking range, and the injection seed is tuned inside the locking range. When the frequency of the master laser is outside the locking range, the injection seed is regeneratively amplified by the slave laser. In this case, light at frequencies ω_1 and ω_0 exist at the output of the slave laser. Chaotic behavior i.e. beating between the slave and master laser frequencies, are observed close to the edges of the locking range.

When the frequency of the master laser is within the locking range, the slave laser follows the master laser. Except for the case of semiconductor lasers where the coupling between gain and refractive index results in a change of output power of the injection locked slave laser by detuning frequency, the output power of an injection locked laser within the locking range is clamped at a fixed value.

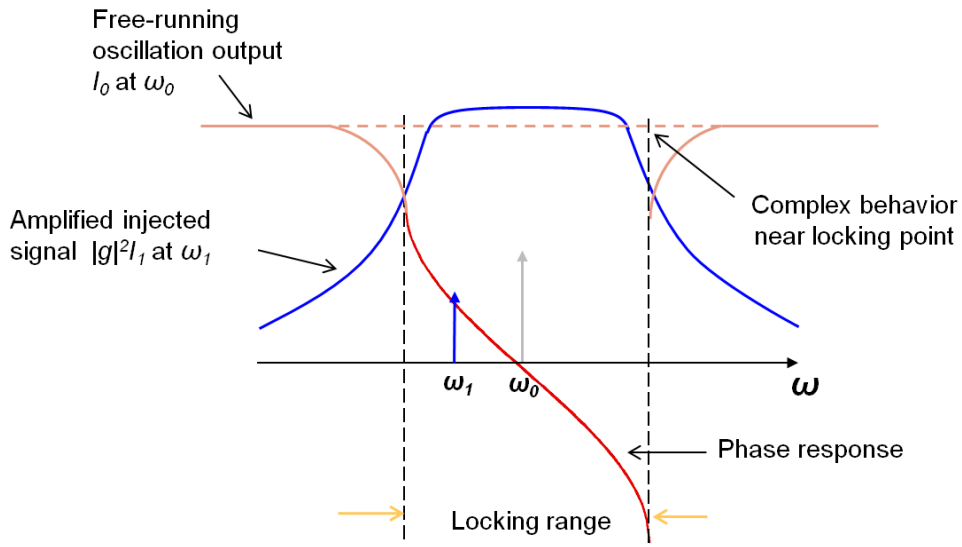

Figure 1.2. Behavior of the slave laser when the injection seed is tuned inside or outside the locking range [3].

Another important property of the injection-locked slave laser is the phase response which was first described by Adler [2]. Adler showed that in weak injection regimes, the phase response of an injection-locked oscillator is an arcsine function of the detuning between master and slave lasers frequencies. The phase response of the injection-locked slave laser within the locking range is also shown in Figure 1.2. Again, in the case of semiconductor lasers, the phase response might deviate from the ideal arsine function due to carrier density dependent refractive index. A detailed study of the output power and phase response of an injection-locked semiconductor laser is presented in Chapter 2.

1.2 Applications of injection locked lasers

Starting in the 1980s, when well-engineered semiconductor lasers became available, injection locking between two lasers, was actively researched [4–6], and proposed for applications such as receiver end design in optical coherent communication [7]. Injection locking of a continuous wave (CW) semiconductor laser has been suggested as an effective method to reduce laser noise [8] and optical linewidth [5]. When the slave semiconductor laser is directly modulated, injection locking is used to reduce the frequency chirp [9][10], increase the frequency response [11], and reduce the nonlinear distortions [12].

In this work, two novel applications of injection locked semiconductor lasers which are taking advantage of the phase properties of an injection-locked laser are introduced. The first application, which will be covered in detail in Chapter 2, is a resonant cavity linear interferometric intensity modulator. It will be shown that this modulator has an inherent linear response, very low V_π (in the order of 1 mV), multi-gigahertz modulation bandwidth, and possible overall optical gain. The key to the perfect linear response of this modulator is the arcsine phase response of the injection-locked laser. This modulator can improve the performance of the existing analog links such as remote antenna (see Figure 1.3) and RF sensor systems, by improving the efficiency and minimizing the distortion of the signal due to its very low V_π and perfect linear response.

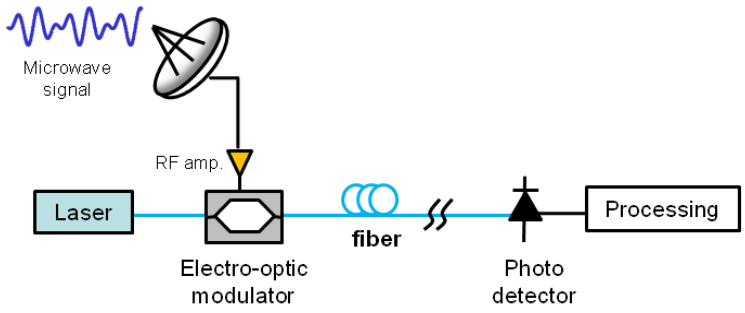

Figure 1.3. Analog link in a remote antenna system.

Other than the conventional analog links, a perfect linear intensity modulator can be useful in analog links with more complex modulation formats such as subcarrier multiplexing (SCM) systems. In a SCM system, multiple microwave subcarriers are combined and placed on a single optical carrier using an optical intensity modulator. To achieve bandwidths in excess of 1 THz, SCM is usually used in combination with time division multiplexing (TDM) or wavelength division multiplexing (WDM). Figure 1.4. shows a block diagram of a multichannel SCM-WDM system. The linearity of the optical intensity modulator is critical for the overall performance of such system. Any nonlinearity of the transfer function of the modulator can cause interband distortion and can affect the recovery of the signal at the receiver end.

Orthogonal frequency-division multiplexing (OFDM) is one of the new and widely used modulation formats in broadband wired or wireless communication systems. An OFDM system is a special kind of SCM system where the subcarrier frequencies are mathematically orthogonal [13]. The orthogonality of the subcarriers removes the need for the frequency guards resulting in higher number subcarriers (higher bandwidth).

Similar to SCM, the performance of an optical OFDM system also depends on the linearity of the response of the modulator since any nonlinearity in the response of the modulator can cause inter-channel crosstalk [14].

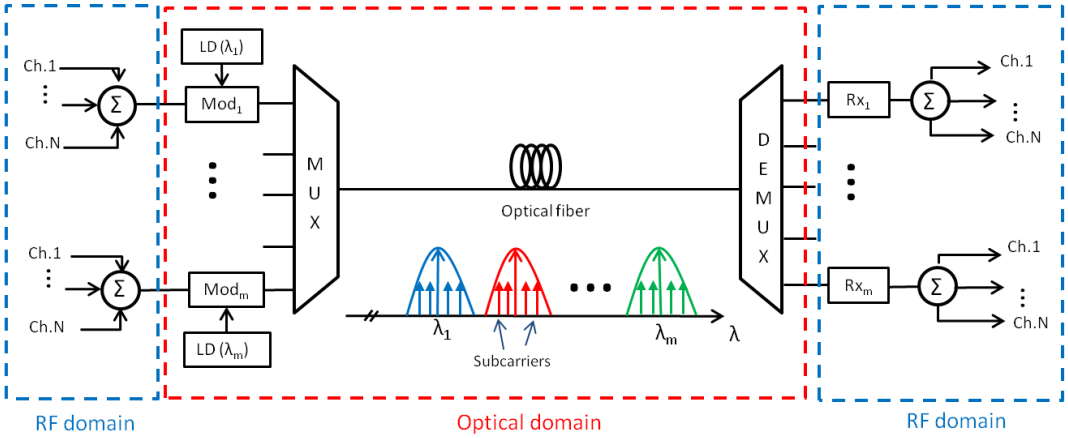

Figure 1.4. Block diagram of a SCM-WDM system.

Another example of systems that can take advantage of a linear intensity optical modulator with a very low V_π is an opto-electronic oscillator (OEO). A diagram of a conventional OEO is shown in Figure 1.5. Due to the high V_π of the electro-optic modulators typically used in OEOs, an RF amplifier is required in the OEO loop. The RF amplifier can be removed by using a modulator with a low V_π that can result in a reduction of the phase noise of the generated RF signal.

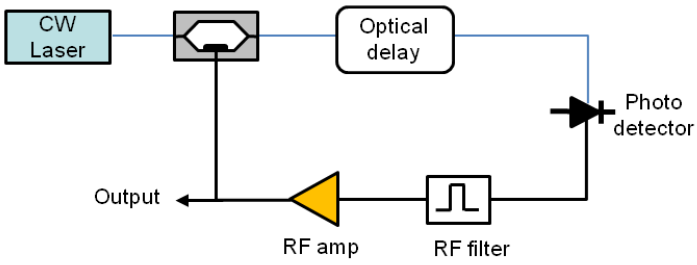

Figure 1.5. Block diagram of a conventional OEO.

Second novel application of an injection-locked semiconductor laser presented in this work, is a direct demodulator and channel filter for phase modulated analog optical signals. This functionality of an injection-locked semiconductor laser will be discussed in detail in Chapter 3. This technique can be used to demodulate phase modulated light without a local oscillator. A design for a reconfigurable cross connect switch which uses arrays of injection-locked semiconductor lasers both as direct phase detector and linear modulators is also proposed. By using the proposed cross-connect switch, information from any wavelength can be arbitrary switched between channels at a rate approaching channel spacing.

In Chapter 4, the focus of the document then shifts to the measurements of the phase noise added by an injection-locked semiconductor laser. The measurements have been done using self-heterodyne technique. The dependency of the added phase noise on the injection power and the frequency detuning is experimentally investigated.

Finally, Chapter 5 discusses possible future works including an on-chip design for the resonant cavity linear interferometric modulator where the gain and the phase

modulating element are separated and a linear interferometric modulator design for pulsed light.

CHAPTER 2: RESONANT CAVITY LINEAR INTERFEROMETRIC INTENSITY MODULATOR

2.1 Introduction

In this chapter a novel optical intensity modulator based on injection locking of a resonant cavity with gain with a linear transfer function, multi-gigahertz bandwidth, possible optical gain, and very low V_π will be presented. The arcsine phase response of the injection locked resonant cavity placed in one arm of a Mach-Zehnder interferometer is the key to the true linear performance of this modulator. 10-dB bandwidth of 5 GHz, V_π of ~2.6 mV at DC and spur-free dynamic range (SFDR) of ~120 dB.Hz$^{2/3}$ are achieved from such modulator with a vertical cavity surface emitting laser (VCSEL) as the resonant cavity with gain.

This chapter is organized as follow: first, the widely used external and direct intensity modulation techniques are discussed. Then, linearized external modulators are introduced and different linearization design and processing techniques, both optical and electrical, are discussed. Next, the resonant cavity linear interferometric intensity modulator is introduced. Simulation results of the performance of the linear modulator with a semiconductor laser as the resonant cavity with gain are presented. Finally, the experimental results of the linear modulator implemented using a multi-mode Fabry-Perot laser and a fiber-coupled VCSEL are presented and compared with the theoretical predictions.

2.2 Intensity modulation techniques

Modulation of light is the process of altering one of the electro-magnetic wave variables in accordance with the variation of a second signal, typically one with a lower frequency. This variable can be the optical intensity, field amplitude, phase, frequency or polarization [15]. Optical communication systems can be classified based on the modulation scheme used for encoding information: intensity modulation or field modulation. Optical systems that use field modulation have a very wide spectral band and require coherent detection. However, coherent detection systems are difficult to implement. As a result, a wide range of commercial communication systems are still using intensity modulators for encoding information. The following sections discuss the applications and different types of existing intensity modulation techniques. Modulation of light intensity can be done by direct modulation of a diode laser or by use of an external modulator device.

2.2.1 Direct modulation of light intensity

Direct modulation is often the easiest way to obtain intensity modulation. Intensity modulation is achieved by directly modulating the pump or injection current of a laser [16]. RF signal modulates the pump current of the laser, which causes modulation of the intensity of the output of the laser. Modulation bandwidth is the main problem for direct modulation of lasers, except for the case of semiconductor diode lasers that their bandwidth can exceed 20 GHz. Higher modulation bandwidths up to 80 GHz have been shown by injection locking of a semiconductor diode laser at high injection regimes [17] .

Moreover, direct modulation of semiconductor lasers has the advantage of the monolithic integration of the laser and the modulation electronic circuit. However, frequency modulation of the output signal or chirp, due to the coupling between gain and refractive index is a disadvantage of direct modulation of laser diodes. Another issue with direct modulation is the nonlinearity of the response of semiconductor lasers. The dynamic response of semiconductor lasers is governed by the intrinsically nonlinear rate equations[18]. The intermodulation distortion is larger when their frequency is closer to the relaxation oscillation of the diode laser. Another source of nonlinearity in directly modulated diode lasers is the nonlinearity of the L-I curve.

2.2.2 External modulation of light intensity

There are two main categories of external modulators: electrooptic modulators and electro-absorption modulators. This classification is based on the material properties used to modulate the light intensity. It should be noted that, in comparing different modulators, there are several important characteristics that need to be considered: the required voltage for π phase shift or V_π, the optical power-handling capability, the linearity of the transfer function, and the environmental stability.

2.2.2.1 Electrooptic modulators

Electro-optic modulators are based on the linear electro-optic effect which is the change of index of refraction of material by applying voltage. This effect is also called the Pockel effect[19]. These modulators are built with crystals that do not possess

inversion symmetry. They can also be made from semiconductor lasers or organic polymers. An electro-optic modulator using a bulk crystal is shown in Figure 2.1.

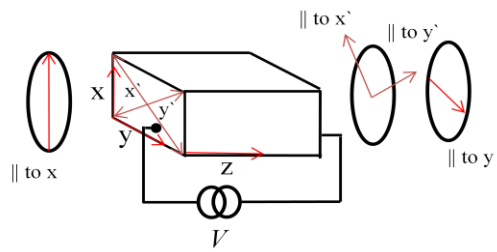

Figure 2.1. A typical electro-optic intensity modulator. A Pockel cell is placed between two crossed polarizers.

The crystal is placed between two crossed polarizers. The total retardation is the sum of the fixed retardation due to the crystal and the electrically induced one. With the electric field off, the crossed output polarizer block off the beam and with the electric field on the optical beam passes through unattenuated. The output intensity as a function of the applied voltage is:

$$I_{out} = I_{in} \sin^2(\frac{\pi}{2}\frac{V}{V_\pi}) = \frac{1}{2}[1+\sin\{\pi\frac{V_m}{V_\pi}\sin(f_m t)\}] \tag{2.1}$$

where V_m is the peak-to-peak voltage of the modulating signal and f_m is the frequency of the modulating signal. If the value of V_m is very small compared to V_π, Equation (2.1) can be rewritten as:

$$I_{out} \approx \frac{I_{in}}{2}[1+\pi\frac{V_m}{V_\pi}\sin(f_m t)] \tag{2.2}$$

Equation (2.2) shows that the output transmitted intensity is a linear function of the RF modulating voltage if the peak-to-peak voltage of the RF modulating signal is very small, as shown in Figure 2.2.

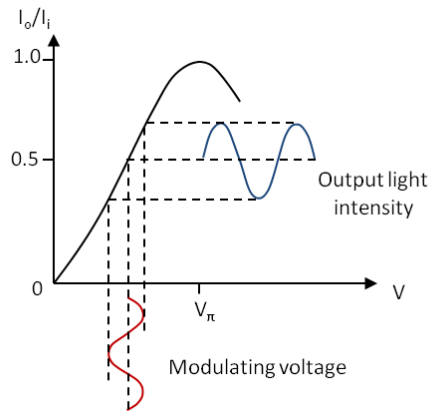

Figure 2.2. Output modulated light intensity versus the modulating voltage of an electro-optic modulator.

The most developed electro-optic modulator is the lithium-niobate ($LiNbO_3$) Mach-Zehnder intensity modulator. Intensity modulation is achieved by placing phase modulator i.e. a lithium-niobate crystal with applied voltage, in an arm of a Mach-Zehnder interferometer. A schematic of an integrated Mach-Zehnder intensity modulator is shown in Figure 2.3. This device has been studied and engineered for over 30 years. Lithium-niobate is a very stable material and Ti-indiffusion offers a well-controlled method for making stable low-loss optical waveguides that can be coupled to fiber with very little loss [20]. Lithium- niobate modulators have a high optical power-handling and respond to frequencies higher than 100 GHz. The typical insertion loss value for

commercially available lithium-niobate modulators is between 3-7 dB. In addition, these devices have a small temperature and wavelength dependence. As it mentioned above, these modulators can respond to high frequencies, but this comes in expense of a high V_π. A broadband modulator with 3 dB bandwidth of 70 GHz and V_π of 5.1 V is demonstrated in [21]. At low frequencies (<500 MHz), a lithium-niobate modulator can achieve V_π<1 V. The record for this is V_π =0.18V at 30 MHz [22].

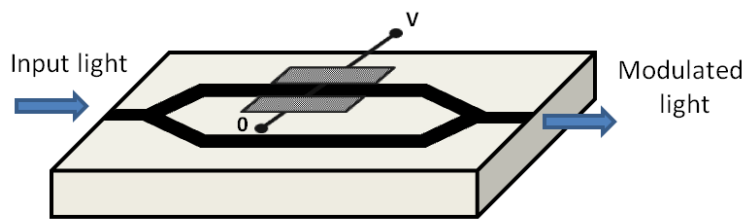

Figure 2.3. An integrated Mach-Zehnder optical intensity modulator.

Transfer function of a lithium-niobate modulator, or any Mach-Zehnder intensity modulator, can be described by Equation (2.3) where Δφ is the phase modulation term. As Equation (2.3) shows, the response of the modulator is not a linear function of the applied voltage.

$$I_{out} = \frac{I_{in}}{2}[1 + \cos(\Delta\phi)] \tag{2.3}$$

The inherent nonlinearity of the lithium-niboate modulators limits the SFDR of the modulator. SFDR is the dynamic range of the signal before the spurious harmonics of

the signal distorted the original signal. In order to measure this quantity, the RF modulating signal should consist of two fundamental frequencies (f_1 and f_2) with equal peak-to-peak voltages. SFDR is the signal-to-noise ratio (SNR) without observation of measurable distortion products above the noise floor of the system [23]. The second-order intermodulation frequencies are $f_1 \pm f_2$ and the third-order intermodulation frequencies are $2f_1 \pm f_2$ and $2f_2 \pm f_1$. Depending on the system bandwidth, the second-order or third-order SFDR is measured. Second-order SFDR is usually measured for systems with bandwidths more than one octave. But in suboctave systems, third-order SFDR is the concern since the second-order intermodulation products fall out of the passband of such systems. In this work we are only considering the third-order SFDR. Typically SFDR of a system is not measured directly but it is calculated from a plot of the fundamental and third-order intermodulation powers in the photodetected power spectrum as a function of modulator input RF power. The SFDR is calculated by fitting two lines with slope of 1 and 3 (in log scale) to the fundamental and third-order intermodulation data sets respectively and extrapolating them to the noise floor of the system. Figure 2.4 shows graphically how the third-order SFDR is calculated using this method.

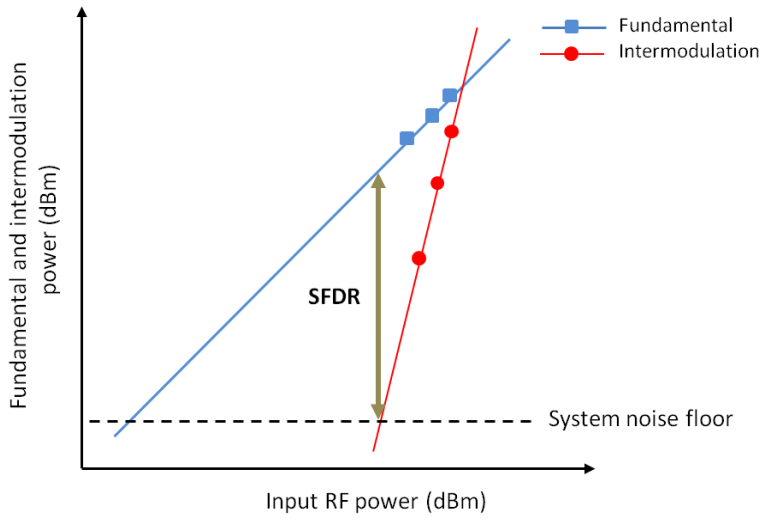

Figure 2.4. Calculation of SFDR from the fundamental and third-order intermodulation power vs. input RF power plot.

The SFDR of a system depends on the instantaneous bandwidth because it affects the output noise level. It also depends on the relationship of the intermodulation output power to the fundamental input power. The third-order distortion varies as the cube of the input RF power, which leads to an SFDR that depends on the instantaneous bandwidth to the 2/3 power. For a perfectly linear modulator, SFDR is the maximum SNR of the system and can be limited by thermal noise, shot noise or intensity noise. The maximum SNR under thermal noise-limited detection is:

$$SNR_{\max} = 10\log(\frac{1}{2} I_D^2 R_s) - 10\log(kT_0) \tag{2.4}$$

If the system is shot noise-limited the maximum SNR is given by:

$$
\begin{aligned}
SNR_{\max} &= 10\log(\frac{1}{2} I_D^2 R_s) - 10\log(2qI_D R_s) \\
&= -6dB + 10\log(\frac{I_D}{q})
\end{aligned}
\tag{2.5}
$$

Finally, if the maximum SNR is limited by relative intensity noise (RIN), the SNR is:

$$
\begin{aligned}
SNR_{\max} &= 10\log(\frac{1}{2} I_D^2 R_s) - 10\log(I_D^2 RINR_s) \\
&= -3dB - RIN(dB)
\end{aligned}
\tag{2.6}
$$

where I_D is the average detector current, R_s is the impedance of the source. Maximum possible SNR of a link as a function of the average photodiode current is shown in Figure 2.5 for a system with -155 dBc/Hz RIN. It can be seen that for photodiode currents below 0.2 mA the SNR of the system is thermal noise-limited. For average photocurrents between 0.2 and 1 mA, the SNR is shot noise-limited. The RIN of the system is limiting the maximum achievable SNR at average photocurrents above 1 mA.

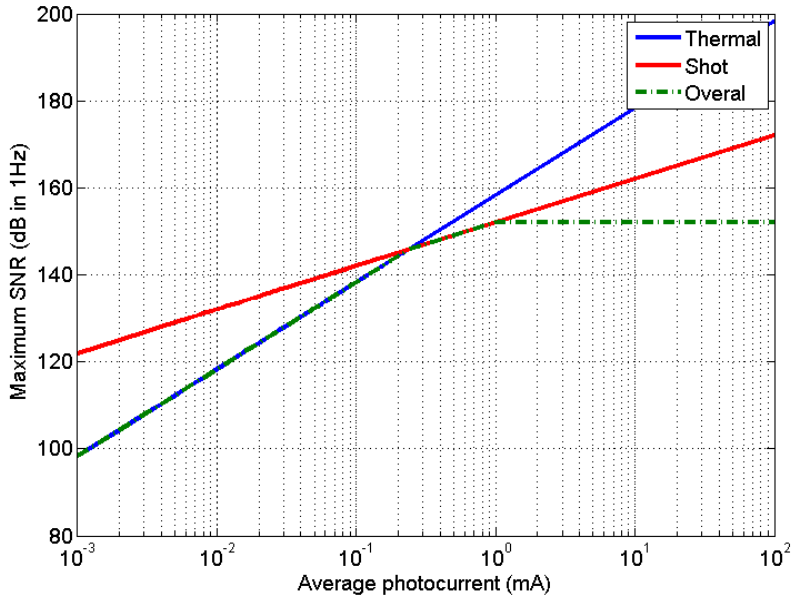

Figure 2.5. Plot of maximum achievable SNR as a function of average photocurrent. Thermal noise and shot noise limits are shown in blue and red lines, respectively. The green line is the maximum achievable SNR for a system with -155 dBc/Hz RIN.

The limited SFDR of a Mach-Zehnder modulator limits the dynamic range of the analog links where these modulators are used in. This can be improved by using linearized modulators, described in the next sections, instead of the conventional lithium-niobate modulators. As an example, SFDR value of ~120 dB $^{2/3}$ Hz at 3 GHz has been reported in [24].

As it mentioned above, electro-optic modulators can be made with semiconductor or organic polymers. Broadband (>30 GHz) electro-optic modulators based on semiconductor materials have been developed [25][26]. However, these modulators have a high V_π because of the relatively low electro-optic coefficient of semiconductors. In

addition to high V_π, the fiber-coupled insertion loss of is high (up to 10 dB). Broadband electro-optic modulators using polymers have been reported as well [27]. Low V_π broadband (up to 100 GHz) polymer modulators are commercially available.

2.2.2.2 Electro-absorption modulators

Electro-absorption modulators (EMAs) are made of either bulk semiconductors by incorporating the Franz-Keldysh effect, i.e. the absorption edge in semiconductors shifts towards longer wavelengths (red shift) in presents of an applied electric field, or quantum-well structures based on quantum-confined Stark effect (QCSE)[16].

EMAs are sensitive to temperature, wavelength, optical power, device design and require a lot of engineering to be commercially feasible. Their main advantage is their low V_π. V_π as low as 0.36 V at DC to >20 GHz has been reported [28][29]. However the maximum optical power that this modulator can handle is less than 2 mW. The V_π increases for optical powers more than this value. For example V_π increases to 1.1 V to be able to handle 60 mW of optical power. Because of the limited optical power-handling of EMAs at high frequencies, EMAs have limited SFDR and is typically less than SFDR of Mach-Zehnder modulators. Another disadvantage of the EMAs is the high fiber-coupled insertion loss that is typically between 10-20 dB.

2.3 Linearized modulators

Nonlinearity of the conventional Mach-Zehnder modulators response poses problems for modern analog broadband data transmission links. In order to improve the

analog links performance by using spectrally efficient modulation formats, high dynamic range modulators are required.

The concept of a linearized modulator i.e. a modulator with a linear transfer function, has gained a lot of attention in the last two decades. Several electronic linearization schemes have been proposed, such as pre or postdistortion and feedforward linearization techniques. All these techniques are required additional electrical and/or optical components, which makes them less cost effective and complicated to implement. The basic operational concepts of some of the linearization techniques are explained in the following sections.

Other than electronic linearization schemes, several optically linearized modulator architectures have been proposed to suppress the third-order nonlinear distortion such as dual or single ring resonator assisted Mach-Zehnder modulator [30][31], dual-signal Mach-Zehnder interferometer modulator [32][33] and, directional coupler with two passive bias [34]. Detailed description of the design and performance of the existing linearized modulators are described in the following sections.

2.3.1 Predistortion linearization scheme

Predistortion is a linearization technique that improves the linearity of the response of an external modulator or a directly modulated laser diode by imposing distortion on the modulating RF signal. An example of a block diagram for a predistortion linearization scheme is shown in Figure 2.6 [35].

An algorithm calculates the required electrical distortion so that the output optical signal of the modulator will be undistorted. This algorithm can be very complicated for

modulators without a well-known transfer function such an EAM. EMA's transfer function depends on several parameters such as modulator length, the number of quantum wells and their thickness etc.[36]. This makes predicting the transfer function of the modulator more difficult. Depending on the system requirements, the required a predistortion algorithm can be different. The predistortion can be adaptive, although the adaptive capability required a more complicated implementation of the predistortion block.

Predistortion linearization technique is an efficient way for linearization at low frequencies however, the performance of this technique degrades at high instantaneous bandwidths. For example in the proposed adaptive predistortion circuit in [35], the suppression of the third-order distortion reduced from 22.1 dB at 6-MHz bandwidth to 9.8-dB suppression at 180-MHz bandwidth for externally modulated links employing a $LiNbO_3$ Mach-Zehnder modulator. It can also be computationally intensive and real-time implementation might not be possible for high bandwidth data.

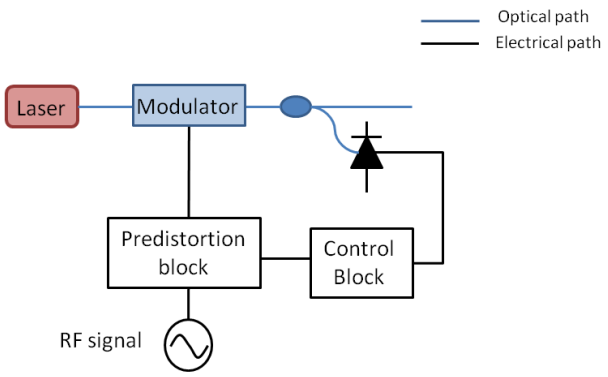

Figure 2.6. Predistortion linearizer system[35].

2.3.2 Feedforward linearization scheme

Feedforward linearization technique is another well-known method used for linearizing the nonlinear response of commonly used Mach-Zehnder modulators. In a feedforward system, an error signal is generated by comparing the original modulating signal with the photodetected output signal of the modulator with proper phase. Then, the amplified error signal is used to modulate a second modulator. Combining the output of these modulators with proper phase results in a signal with no distortion [37][38]. A simplified diagram of a feedforward linearization scheme is shown in Figure 2.8.

The performance of a feedforward linearization system is dominated by amplitude and phase matching between the optical signals. SFDR improvement of only 6 dB is achieved by using a feedforward linearization technique in [37].

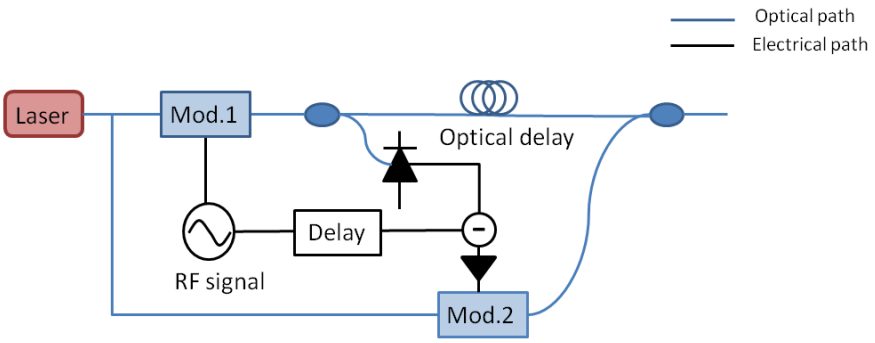

Figure 2.7. Block diagram of a feedforward linearization system.

2.3.3 Linearized ring resonator assisted Mach-Zehnder modulators

A ring resonator assisted Mach-Zehnder modulator (RRMZM) is a Mach-Zehnder modulator with a ring resonator in one of the modulator arms. The ring resonator works

as a phase modulator when an electrical signal is applied to it which changes the refractive index of the ring. Several designs of linearized RRMZMs have been proposed in literature [29] [30][39]. The linearization can be realized by using two ring resonators in push-pull configuration such as the one proposed in [31]. By carefully designing the coupling coefficients between the ring resonators, the Mach-Zehnder interferometer and the RF drive signal amplitude split ratio between the rings, a highly linear performance can be achieved. Figure 2.8 shows a schematic of a resonator assisted Mach-Zehnder modulators with two ring resonators. A hybrid modulator has also been proposed which has a $LiNbO_3$ crystal as a phase modulator and a ring resonator as a phase filter. the ring resonator has an arctan phase response is the key feature for the predicted high SFDR of the modulator proposed in . Figure 2.9 shows a schematic of the proposed ultra-linear modulator in [30]. A high SFDR (147 dB) has been predicted for the proposed modulator in [30] however, no experimental result has been shown.

Although, high SFDRs have been predicted for linearized RRMZMs, there are few challenges regarding the fabrication of these devices. To achieve high bandwidth, ring resonators with very small diameter should be fabricated. Fabrication of low loss micro-ring resonators is not straight forward. Moreover, to achieve a linear response of such modulators, the coupling between the ring resonator and the interferometer is critical. This can not only make the fabrication process more challenging but also can made the performance of the device more sensitive to the operating conditions (temperature, etc.).

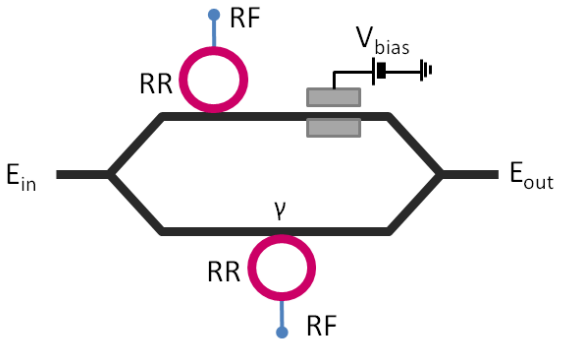

Figure 2.8. Schematic of a dual RRMZM optical intensity modulator in push–pull configuration [31].

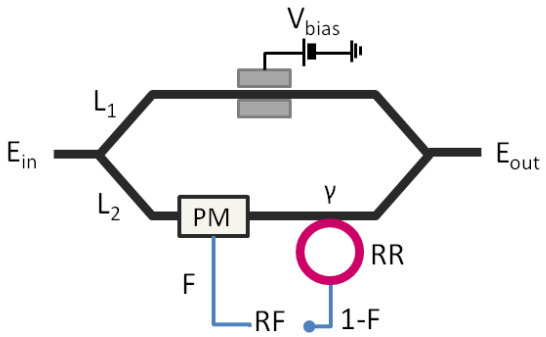

Figure 2.9. A hybrid RRMZM modulator. γ is the coupling coefficient of the ring resonator. The phase modulator and the ring resonator are driven by the same RF signal with a power split ratio of F and 1-F[30].

2.3.4 Dual parallel Mach-Zehnder modulator

A dual parallel Mach-Zehnder modulator is a Mach-Zehnder interferometer with a Mach-Zehnder modulator in each arm [32][40][41]. One modulator serves as the modulation element and the other one as the compensation element. A schematic of a

dual parallel Mach-Zehnder modulator demonstrated in [32] is shown in Figure 2.10. The optical and electrical input signals are split unequally between two Mach-Zehnder modulators. Both of the Mach-Zehnder modulators remain biased at quadrature, therefore no even-order harmonic distortion is generated in either modulator. The adjustable parameters for this type of modulator are the split ratios of the RF and optical signals. The exact values of these parameters to achieve a desired level of nonlinearity distortion suppression are calculated from the Taylor expansion of the modulator transfer function. The relative phases of the modulation signals need to be adjusted so that the intermodulation products exactly cancel out. Although the intermodulation distortions do subtract, in practice, they do not completely cancel out. This imperfection is due to the required tight control of the adjustable parameters which can be challenging to implement in the laboratory conditions. The signal level from this modulator is typically below that of a single Mach-Zehnder modulator, but the dynamic range can be improved [42].

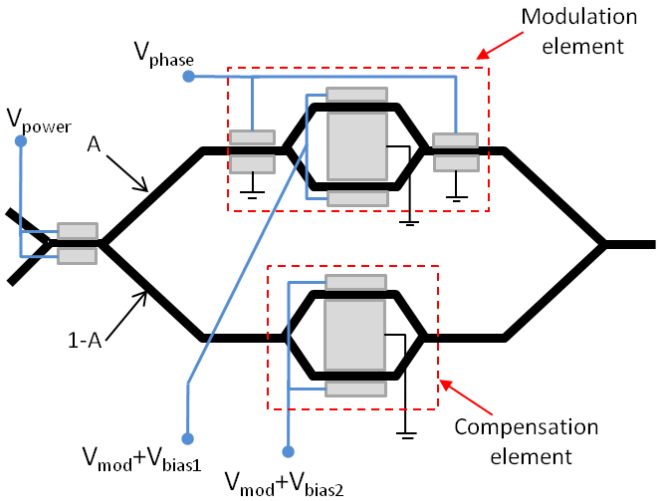

Figure 2.10. Schematic of a dual parallel Mach-Zehnder modulator [32].

2.3.5 Cascaded Mach-Zehnder modulators

Cascaded Mach-Zehnder modulators or dual series Mach-Zehnder modulators are similar to dual parallel Mach-Zehnder modulators described above [33]. Again, the two Mach-Zehnder modulators are biased at their half-voltage to avoid even-order distortion generation and there is a RF split between them. But, there is no input optical power split since the modulators are cascaded, see Figure 2.11. Again, it should be emphasized that although both cascaded and dual parallel Mach-Zehnder modulators can achieve high SFDR, the implementation of these devices is a complicated process and they require precise and active control of the voltages [42].

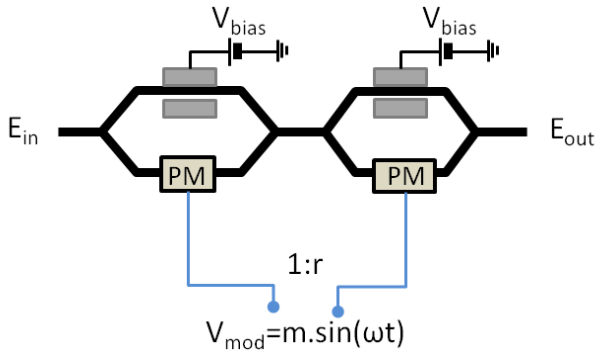

Figure 2.11. Schematic of a cascaded Mach-Zehnder modulator[33].

2.3.6 Directional coupler with two passive biases

This modulator is a simple directional coupler modulator but with three electrode sections. The first section is where the RF modulating signal is applied and followed by two passive or DC-biased electrode sections [34][43]. A schematic of this modulator is shown in Figure 2.12. The first section is fed with the optical input to one arm only and

biased where its second harmonic is zero. The outputs from the two arms of this section are complementary. The two passive sections create a relative power split and phase shift between these two modulated signals. By adjusting these parameters the third-order intermodulation distortions can potentially go to zero. The high electrical power consumption of this device is the main drawback of this design [34].

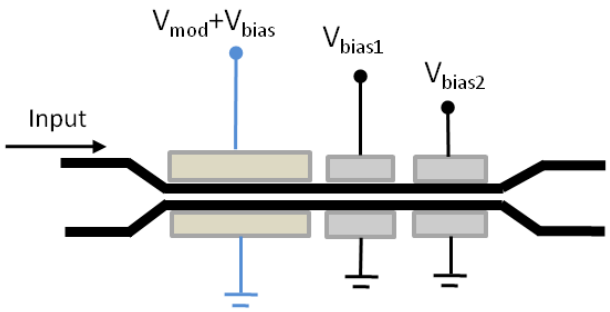

Figure 2.12. Schematic of a directional coupler with two passive biases [43].

So far in this Chapter, the most common linearization techniques for external modulators and linearized modulators are briefly discussed. The discussed linearization techniques require additional electrical or optical components that make them less cost effective. Moreover, the proposed and in some cases demonstrated optically linearized modulators, such as resonator-assisted modulators, dual-signal Mach-Zehnder interferometer modulators, and linearized directional couplers, yet have a limited reduction of the intermodulation products and require a tight control of the device parameters such as length, applied voltages, and coupling ratios which, make the device fabrication challenging. Also, most of these designs have a higher V_{π} and insertion loss than conventional modulators.

A high-speed intensity modulator that has an inherent linear transfer function without sacrificing the optical power handling capability or drive voltage sensitivity can greatly improve the performance of optical analog data transmission links [20] and play a crucial role in next generation OFDM networks [44]. A new external modulator design is required since the modulators currently used in optical links cannot offer all the above characteristics. In the following section, an intensity modulator with a pure linear response which is inherent in the design i.e. no additional linearization scheme is required, based on an injection locked resonant cavity is introduced.

2.4 Resonant cavity linear interferometric intensity modulator

A resonant cavity linear interferometric intensity modulator is a novel modulator for achieving a perfect linear modulator transfer function without a complicated linearization technique[45]. The key to the perfect linear response is in the use of an arcsine phase modulator placed in one arm of a Mach-Zehnder interferometer. The arcsine phase modulator is a resonant cavity with gain for example a laser, that is injection locked to the input light to the modulator. According to the steady state solution of the Adler's equation, an injection-locked laser [2], has an arcsine phase response within a frequency range called locking range. The arcsine phase response is a function of the detuning of the resonant frequency from the injection seed frequency, as shown in Equation (2.7).

$$\varphi(\omega_1) = \arcsin\left(\frac{\omega_0 - \omega_1}{\omega_m}\right) \tag{2.7}$$

ω_1 is the injected seed frequency or the input light to the modulator, ω_0 is the cavity resonance frequency and ω_m is half of the locking range. By keeping the injection seed frequency fixed and modulating the frequency of the injection-locked resonant cavity, an arcsine phase modulated light at the output of the injection-locked resonant cavity is obtained. When the arcsine phase modulated light from the injection-locked resonant cavity with gain is combined in quadrature with the reference arm of the interferometer, the resulting total intensity is directly proportional to the signal modulating the resonant frequency of the injection-locked slave laser, *f(t)*, as shown in Equation (2.8).

$$I_{out} = \frac{I_{in}}{2}\left\{1+\cos\left(\arcsin(f(t)) - \frac{\pi}{2}\right)\right\} = \frac{I_{in}}{2}(1+f(t)) \tag{2.8}$$

Except for the case of semiconductor lasers, the output power of an injection-locked resonant cavity is clamped at a fixed value within the locking range [3]. A diagram of this modulator is shown in Figure 2.13.

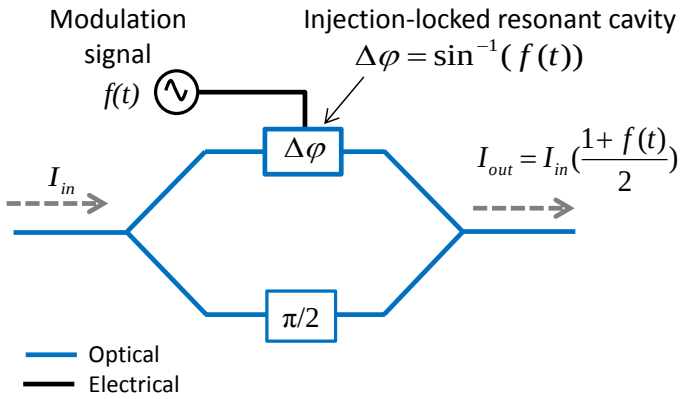

Figure 2.13. Resonant cavity linear interferometric intensity modulator setup.

A simple numerical simulation comparing the SFDR of the proposed linear modulator assuming a perfect arcsine phase modulation with a typical electro-optic Mach-Zehnder modulator is performed. Results are shown in Figure 2.14(a) and (b). Based on the simulation result, the SFDR of the quadrature-biased resonant cavity linear interferometric intensity modulator is higher than the electro-optic Mach-Zehnder modulator at any depth of modulation. As it can be seen, the SFDR of a Mach-Zehnder electro-optic modulator decreases by depth of modulation, which is not the case for the linear modulator. When biased at quadrature, an electro-optic Mach-Zehnder modulator has a SFDR of ~70 dB for 10% depth of modulation while the linear modulator has SFDR of more than 100 dB for the same depth of modulation.

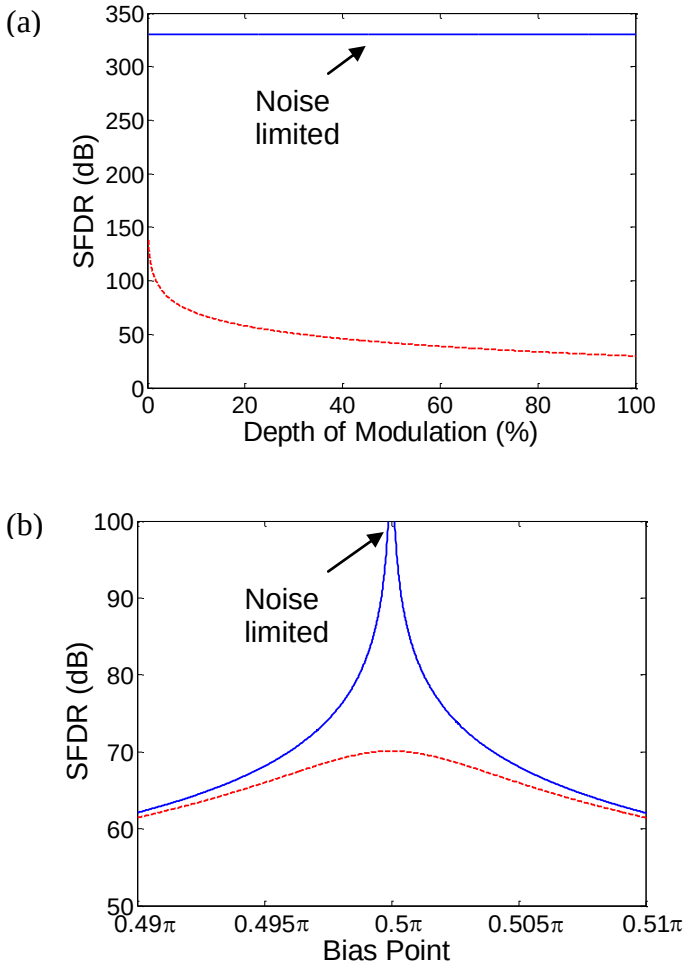

Figure 2.14. Simulation results: (a) SFDR vs. depth of modulation (b) SFDR vs. bias point of the modulator at 10% depth of modulation.

As it mentioned above these simulation results are for an ideal case of a perfect arcsine phase response from an injection-locked resonant cavity with gain. However, as it will be discussed in the following sections, the phase response of injection-locked semiconductor lasers might deviate from the perfect arcsine function due the carrier

density dependent refractive index. Deviation of the phase response from the perfect arcsine function introduces limitations on the achievable SFDR of such a modulator.

Kobayashi and Kimura showed phase modulation of light using an injection locked semiconductor laser [46]. However, in the work presented here, we are demonstrating for the first time, the use of an injection locked semiconductor laser as an arcsine phase modulator to achieve linear intensity modulation. It will be shown in the next section that the linearity of the response of a semiconductor resonant cavity linear modulator does not always follows the ideal case and depends on the resonant cavity and operating parameters. Studying the performance of such a modulator requires a detailed understanding of the performance of an injection-locked semiconductor laser as an arcsine phase modulator.

In the following sections, we first introduce the differential rate equations governing the amplitude, phase and carrier density of an injection locked semiconductor laser. By solving the rate equations in the steady state, the asymmetric change of the output power of an injection locked semiconductor laser is numerically calculated. Then, the phase response of an injection-locked semiconductor laser at different injection ratios and linewidth enhancement factors is studied. Dynamically stable and unstable regions of the locking range are found numerically as well. The calculated phase response within the dynamically stable locking range is then used in calculation of the linear modulator signal-to-intermodulation ratio which is a measure of SFDR. Effects of several parameters on the linearity of the modulator response are studied. These parameters are:

injection ratios, depth of phase modulation, residual amplitude modulation, nonlinearity of the resonant cavity response.

2.4.1 Phase response of an injection locked semiconductor laser

The differential equations describing the electric field amplitude, phase, and carrier density of an injection-locked semiconductor laser are as follow [4][47–50]

$$\frac{d}{dt}E(t) = \frac{1}{2}G_N(N(t) - N_{th})E(t) + \frac{E_1}{\tau_r}\cos(\Delta\omega t - \phi(t)) \tag{2.9}$$

$$\frac{d}{dt}\phi(t) = \frac{1}{2}\alpha G_N(N(t) - N_{th}) + \frac{E_1}{\tau_r E(t)}\sin(\Delta\omega t - \phi(t)) \tag{2.10}$$

$$\frac{d}{dt}N(t) = J - \frac{N(t)}{\tau_s} - G_N(N(t) - N_0)E^2(t) \tag{2.11}$$

where E ,ϕ, N, G_N, τ_r , N_{th}, N_0, τ_s, α and J are the injection-locked semiconductor laser or slave laser electric field amplitude, phase, carrier density, gain coefficient, cavity round trip time, threshold carrier density, transparency carrier density, spontaneous emission lifetime, linewidth enhancement factor and injection current, respectively. E_1 is the master laser electric field that is coupled into the slave laser cavity. Also, $\Delta\omega=\omega_1-\omega_0$ where ω_0 and ω_1 are the angular frequencies of the free running slave and master lasers. Steady state solutions can be found by setting $\phi(t)=\Delta\omega t+\phi_L$, E (t) = E_0 and $N(t)=N_{th}+\Delta N$:

$$\Delta N = -2\frac{1}{\tau_r G_N}\frac{E_1}{E_0}\cos(\phi_L) \tag{2.12}$$

$$\Delta\omega = -\frac{E_1}{\tau_r E_0}(\sin\phi_L + \alpha\cos\phi_L) \tag{2.13}$$

$$E_0^2 = \frac{E_f^2 - \tau_p \Delta N / \tau_s}{1 + \tau_p G_N \Delta N} \tag{2.14}$$

It should be noted that E_f is the electric field amplitude of the free running slave laser and E_0 is the electric field amplitude of the injection locked slave laser. As it can be seen from Equation (2.14) the amplitude of the injection-locked semiconductor laser is different from the free running value. The change of the electric field amplitude of the injection-locked semiconductor laser from the free running value depends on the change of the carrier density. τ_p is the photon lifetime of the resonant cavity. From these solutions and with no approximation on the injection ratio, an equation for the phase response of the injection locked slave laser can be found [47].

$$\phi_L = -\arcsin\left(\frac{\Delta\omega}{\Delta\omega_L}\right) - \arctan(\alpha) \tag{2.15}$$

where $\Delta\omega_L = \frac{E_1}{\tau_r E_0}\sqrt{(1+\alpha^2)}$ is the half locking range of the injection-locked semiconductor laser.

From the definition of the half locking range, it can be seen that the electric field amplitude of the injection-locked semiconductor laser (E_0) has to be known at every detuning frequency to calculate the exact value of the phase shift. Using the steady state

solutions of the change of carrier density, phase and electric field amplitude of the injection-locked semiconductor laser, an equation relating the change of carrier density and amount of frequency detuning is derived [51], see Equation (2.16).

$$\begin{aligned}&\Delta N^3\left[-(1+\alpha^2)\tau_p G_N^2/4\tau_s\right]+\Delta N^2\left[(1+\alpha^2)G_N^2E_f^2/4+\Delta\omega\alpha G_N\tau_p/\tau_s\right]\\&+\Delta N\left[-\Delta\omega\alpha G_N E_f^2-\Delta\omega^2\tau_p/\tau_s-f_L^2E_1^2G_N\tau_p\right]-f_L^2E_1^2+\Delta\omega^2E_f^2=0\end{aligned} \tag{2.16}$$

This cubic equation can be solved numerically. For every value of $\Delta\omega$, there is only one solution that corresponds to a physically possible value for the output electric field of the injection-locked semiconductor laser.

Table 1 shows the list of parameter used to describe the semiconductor laser in our model. Using these values and knowing the exact values of ΔN at each frequency detuning, the output power of the injection-locked slave laser (E_0^2) is calculated. Figure.2.15 shows the normalized injection-locked output power to the free running output power of the slave laser as a function of detuning frequency at fixed injection ratio of 0.02 and α of 1. Here, the injection ratio is defined as the ratio of the injection seed electric field amplitude and free running slave laser electric field amplitude, $R=E_1/E_f$.

Table 1 Laser parameters

Symbol	Quantity	Value
L	Cavity length	1.25 mm
τ_r	Cavity round trip time	2.5×10^{-11} s
τ_p	Photon lifetime	1×10^{-11} s
τ_s	Spontaneous emission lifetime	2×10^{-9} s
G_N	Gain coefficient	1×10^{5} 1/s
n	Index of refraction	3

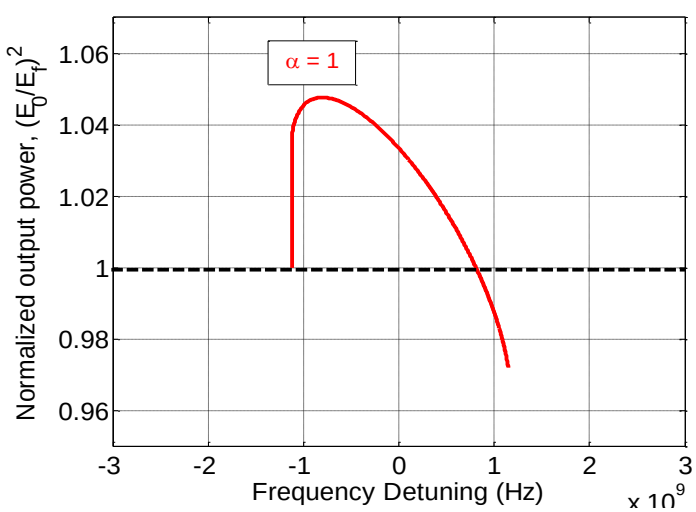

Figure.2.15. Normalized output power of an injection-locked semiconductor laser as a function of frequency detuning (α =1).

As it can be seen in Figure.2.15, the output power of the injection-locked semiconductor laser is not a fixed value and it changes by frequency detuning across the locking range. It should be noted that the change of the output power is asymmetric around the nominal zero detuning frequency. The asymmetric injection locked output power for non-zero α was first studied by Lang [4].

For the semiconductor laser parameters used in the simulation here, the maximum output power is ~5% more than the free running output power near the lower bound of the locking range and the minimum can theoretically be ~3% less than the free running value at the most positive frequency detuning. However, as it will be described below the output powers below the free running value are not physically achievable.

Injecting light from a master laser into the cavity of a semiconductor slave laser reduces the carrier density of the semiconductor laser. Reduction of the carrier density increases the refractive index in the active area of the semiconductor laser that corresponds to a downshift of the resonance frequency of the semiconductor slave laser. The resonant frequency shift is related to the gain, linewidth enhancement factor and change of carrier density and can be described by [48]:

$$\Delta\omega_{cav} = \alpha g \Delta N / 2 \tag{2.17}$$

The shift of the resonant frequency results in a change of the locking range boundaries. The lower limit of the locking range changes from $-E_1/\tau_r E_0$ for α=0 to $-E_1\sqrt{1+\alpha^2}/\tau_r E_0$ for a non-zero α [4]. Similarly, an increase of the upper limit of the locking range from $E_1/\tau_r E_0$ to $E_1\sqrt{1+\alpha^2}/\tau_r E_0$ is theoretically predicted. These

changes of the locking range boundaries results in an overall increase of the locking range of a semiconductor laser with non-zero α by a factor of $\sqrt{1+\alpha^2}$. However, the upper limit of $E_1\sqrt{1+\alpha^2}/\tau_r E_0$ cannot be reached in practice [52]. This can be explained as follow: the output power of an injection-locked semiconductor laser is determined by the phase difference between the master laser and the shifted cavity resonance. Figure.2.16 shows graphically the shift of the cavity resonance and its relative phase to master laser at different points across the locking range. At the lower edge of the locking range, the relative phase is $\cot^{-1}\alpha$, Figure.2.16 (a). At a point that the frequency of master and shifted slave laser overlap, Figure.2.16 (b), the relative phase is zero and they add up in phase. Maximum output power is obtained at this point. After this point, the output power decreases by increasing the detuning between the master and shifted slave laser frequency, Figure.2.16 (c)-(d). At the upper edge of the stable locking range Figure.2.16 (d), the master and shifted cavity resonance are out of phase and the locked output power is equal to the free running value. For master laser frequencies above this point, Figure.2.16 (e), no stable locking can be achieved (chaotic behavior) since based on Equation (2.17) positive change of the carrier density is required to achieve a positive shift of the resonant cavity frequency. This is not physically possible for a fix injection current to the semiconductor laser.

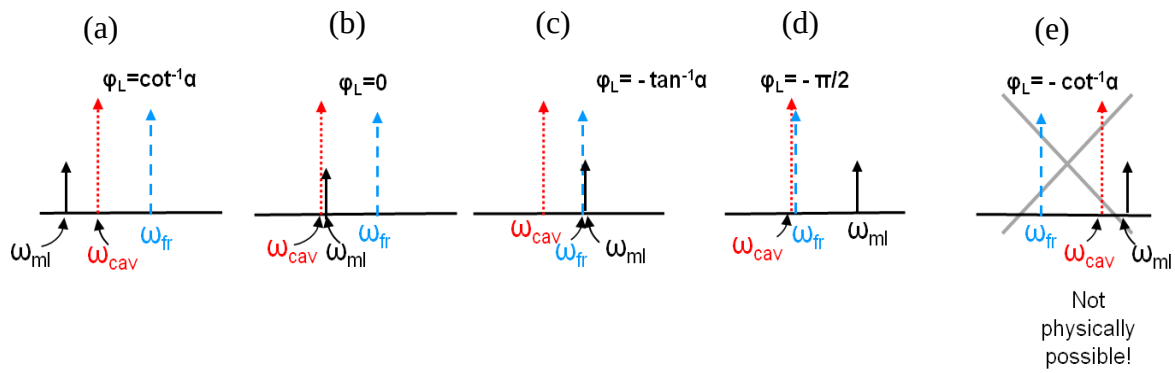

Figure.2.16.Graphical representation of the resonant cavity frequency shift and its relative phase to the master laser at different detuning frequencies across the locking range.

It is shown that the negative carrier density change approximately occurs for detuning frequencies between $-E_1\sqrt{1+\alpha^2}/\tau_r E_0$ and $E_1/\tau_r E_0$ [52]. This means that for a non-zero α, the locking range is asymmetric around the nominal zero detuning. Within this range, the normalized output power of the injection locked semiconductor slave laser is greater than 1.

By knowing the upper and lower limits of the stable locking range, the corresponding range of the phase shift within the stable locking range can be obtained from Equation (2.15). The maximum achievable range of phase shift from an injection locked semiconductor laser is:

$$\cot^{-1}\alpha < \phi_L < -\pi/2 \qquad (2.18)$$

To see the effect of the linewidth enhancement factor on the output power of the injection-locked laser, first the injection-locked laser output power as a function of detuning frequency for α=0 is obtained. Other than α, all the other laser parameters are the same as above. The result is shown in Figure.2.17. It can be seen that the normalized output power of the injection-locked slave laser is symmetric with respect to nominal zero detuning.

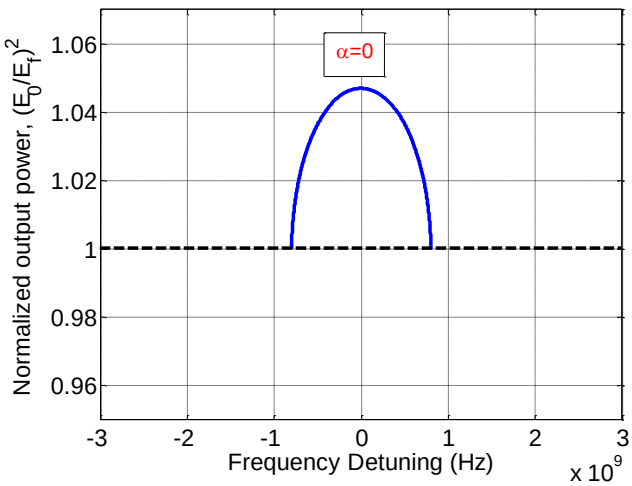

Figure.2.17. Normalized output power of an injection-locked semiconductor laser as a function of frequency detuning (α =0).

In this case the output power of the injection-locked semiconductor laser is higher than the free running power across the entire locking range. The locking range is symmetric and the lower and upper limits are $-E_1/\tau_r E_0$ and $E_1/\tau_r E_0$, respectively. The maximum output power (~5% more than the free running output power) is obtained at the

zero detuning frequency. This can be explained using the phasor diagrams for injection locking of an oscillator [10]. When the injection signal is at resonance frequency (zero detuning) both slave laser and the amplified injection seed electric field vectors are in phase. For non-resonant frequencies, there is a phase shift between slave laser and injection seed electric fields which results in a decrease of the amplitude of the output electric field, see Figure. 2.18.

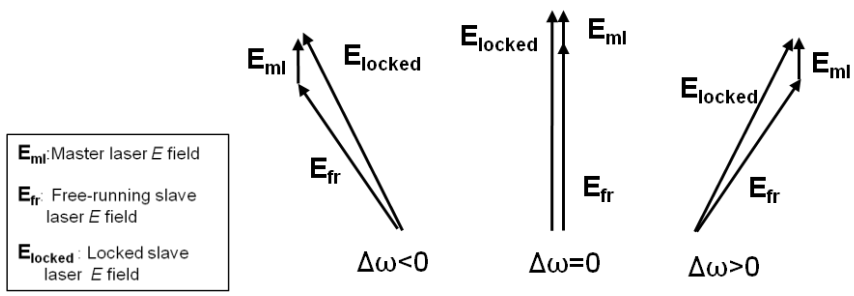

Figure. 2.18. Phasor diagram of the master and slave laser electric fields within the locking range for α=0.

The calculated output power of the injection-locked semiconductor laser as a function of frequency detuning for different values of linewidth enhancement factor, ranging from zero to 3 are compared, see Figure. 2.19. The maximum output power is the same for different values of the line width enhancement factor but the locking range is larger for higher values of α.

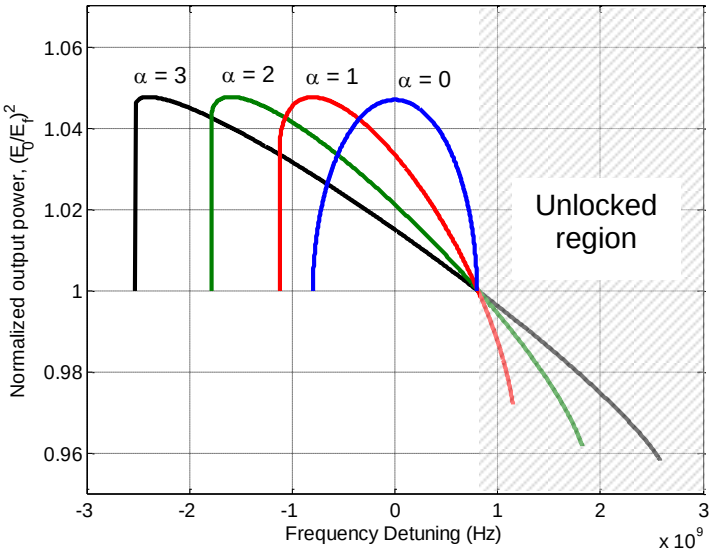

Figure. 2.19. Normalized output power of an injection locked laser for α= 0, 1, 2, and 3.

Next, the steady state phase response of the injection-locked semiconductor laser is calculated using Equation (2.15) the calculated values of the injection-locked laser output power. Figure 2.20 (a) show the steady state phase response of the injection-locked slave laser as a function of frequency detuning at different values of the injection ratio for α=0. It can be seen that the locking range is increasing by increasing the injection ratio but still symmetric around the zero detuning frequency.

Figure 2.20 (b) shows the steady state phase response for α =3. In Figure 2.20 (b) the regions where the normalized output power is below 1 are shown with dashed lines. By comparing Figure 2.20 (a) and (b), it can be seen that a non-zero α results in an asymmetric arcsine phase curve about the nominal zero detuning. Note the shift of the arcsine curve on the vertical axis from 0 in Figure 2.20 (a) to $-\tan^{-1}\alpha$ in Figure 2.20 (b). Also the range of phase shift is $-\pi/2$ to $\pi/2$ for α=0 and $-\pi/2$ to $\cot^{-1}\alpha = 0.1024\pi$ for α=3.

We have also studied the effect of high injection power on the phase response of the injection-locked laser. Figure 2.20 (c) shows the steady state phase response at a high injection ratio (here 1) looks like an arctan function instead of the arcsine at low injection. It should be noted that this effect exist independent of the value of α. This indicates that the desirable operating point for the resonant cavity linear interferometric modulator is at weak injection regimes.

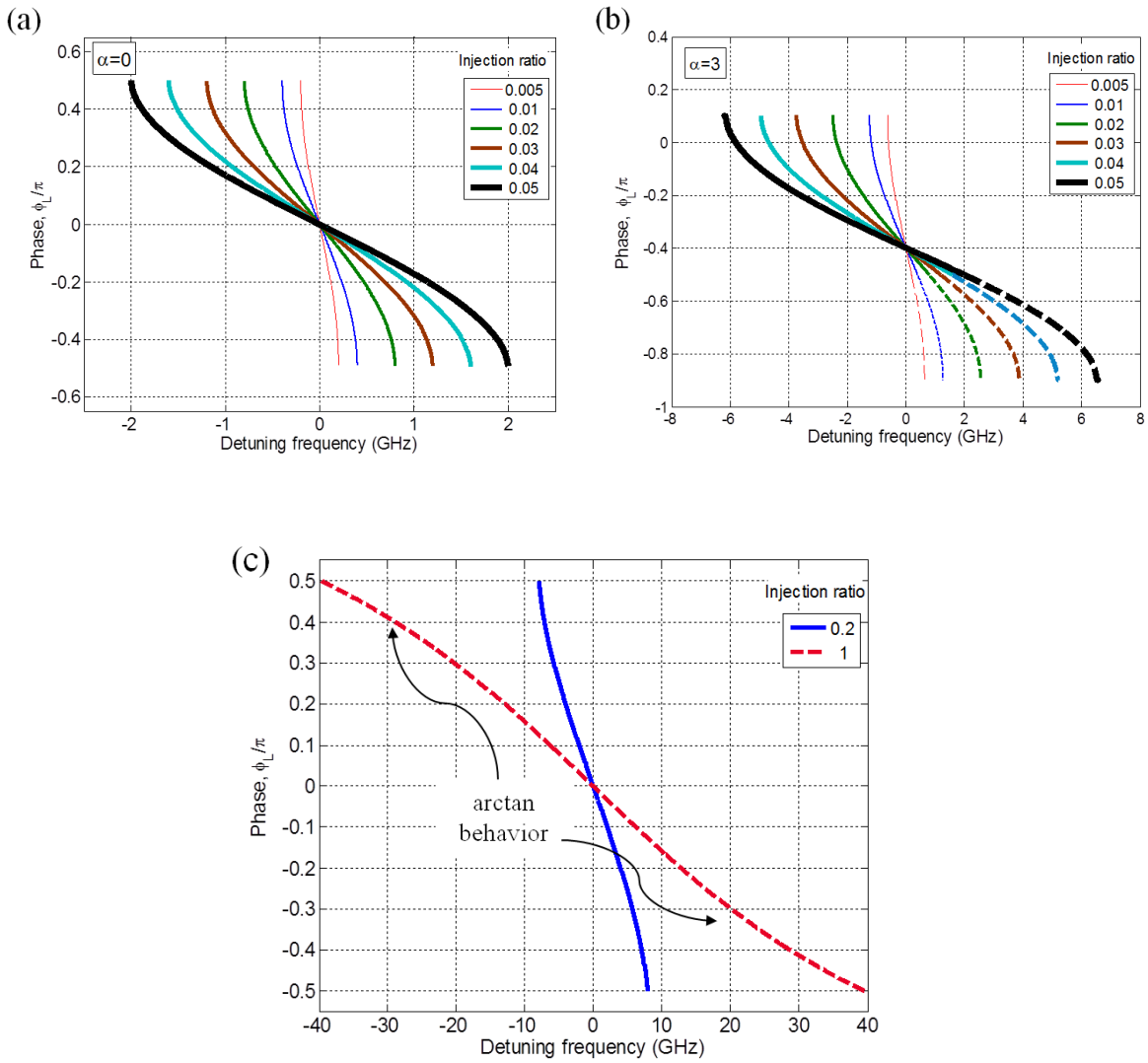

Figure 2.20. Phase vs. frequency detuning for different injection ratios and for (a) α =0 and (b) α =3. The unlocked regions are shown by dashed lines in (b). (c) Phase response of the injection locked laser at a high injection ratio (dash line) looks like an arctan and an arcsine at a low injection ratio (solid line).

2.4.2 Dynamic stability of an injection locked semiconductor laser

According to theoretical study done by Henry et al. [52] in semiconductor lasers, the relaxation oscillation frequency increases with increased frequency detuning. However, the amplitude of the relaxation oscillation is not the same for positive and negative detuning frequencies. For negative frequency detuning, the relaxation oscillation is damped. However, on the positive frequency detuning side the amplitude of the relaxation oscillation increases correspondingly. After a threshold is crossed, the undamped relaxation oscillation causes instability in the form of self-pulsation in the injection locked slave laser.

In order to determine the dynamically unstable region of the locking range, we follow the Mogensen method [47]. The system of differential equations describing the injection locked semiconductor laser is perturbed by a small signal. The equations are then linearized by taking the Laplace transform. Knowing that a linear system is stable when all the poles of the transfer function are at the left side of the complex plane *s*, the dynamic stability plot for different injection ratios can be obtained. Using the parameters listed in Table 1, the stability plot of the injection locked semiconductor laser is numerically calculated. The results are shown in Figure 2.21. It can be seen that for very weak injection ratios (<-14 dB) the entire locking range is stable. As the injection ratio is increased, an unstable region is observed.

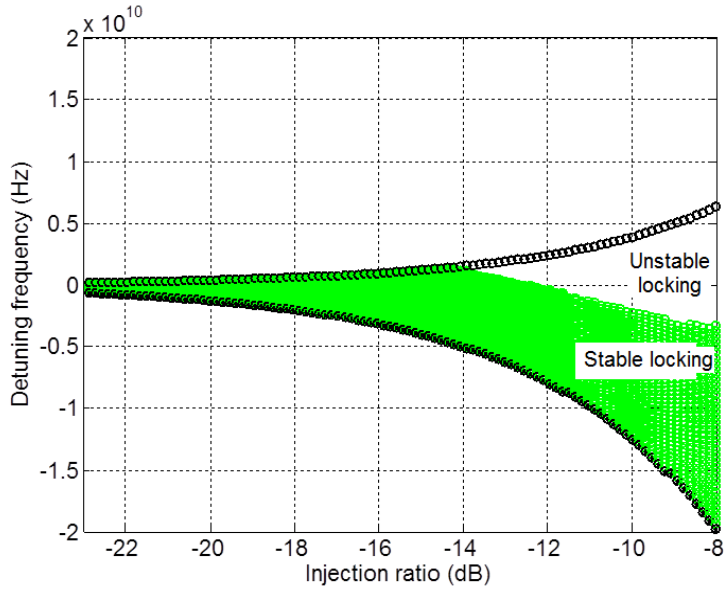

Figure 2.21. Stability plot of an injection locked semiconductor laser with parameters listed in Table 1.

As a result of dynamic instability, the range of the phase shift that can be achieved by detuning the slave laser frequency across the locking range is reduced when the injection ratio exceeds a certain threshold. In Figure 2.21. this threshold is ~ -14 dB. Effects of the asymmetric arcsine phase on the performance of a semiconductor resonant cavity interferometric modulator are studied in the next section.

2.4.3 Linearity of modulator response

As shown in the above section, the alpha parameter and injection ratio determine how the phase response of an injection locked semiconductor laser deviates from the perfect arcsine function which results in a degradation of the linearity of the modulator

response. In addition to the non-zero α and injection ratio, other important parameters in determining the SFDR of this modulator are depth of phase modulation, depth of residual amplitude modulation and linearity of the resonant cavity detuning. In order to study the effects of these parameters on the linearity of the modulator, a numerical model of the modulator using the phase response calculated in the previous section is developed.

In this model, the signal-to-intermodulation ratio of the modulator is calculated in the following manner: the injection locked semiconductor slave laser frequency is modulated at two different frequencies. The modulating signals have equal amplitudes. The phase response at every detuning frequency within the stable locking range is obtained by using the method described in the previous section. Since the response of the semiconductor laser is much faster than the modulation frequencies, the use of the steady state solution of the phase response is appropriate. The output optical intensity of the modulator is obtained by using this phase response in the transfer function of a Mach-Zehnder modulator. The power spectrum is obtained by taking the Fast Fourier Transform (FFT) of the detected output signal. Third-order signal-to-intermodulation ratio is obtained from the ratio of the power of the fundamental frequency to the power of the third order intermodulation frequencies.

The surface plot of the signal-to-intermodulation ratio of the modulator as a function of injection ratio (10^{-8} to 0.01) and depth of phase modulation within the stable locking range (1% to 100%) for a fixed alpha parameter is shown in Figure 2.22. It should be noted that thermal noise, shot noise and relative intensity noise (RIN) are not

included in this model. Also, the simulation results presented in this paper are obtained when the modulator is biased at quadrature.

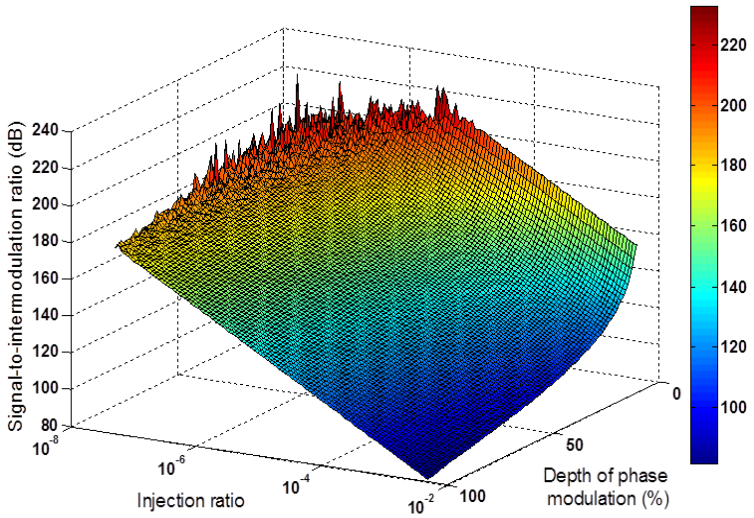

Figure 2.22. Surface plot of signal-to-intermodulation ratio as a function of depth of modulation and injection ratio for α =3.

Figure 2.23(a) and (b) show two cross-sections of above figure. Figure 2.23 (a) is the plot of the signal-to-intermodulation ratio as a function of injection ratio at a fixed depth of phase modulation (40%) and Figure 2.23 (b) shows the signal-to-intermodulation ratio as a function of depth of phase modulation at a fixed injection ratio of 0.1. Figure 2.23 (a) shows that signal-to-intermodulation ratio decreases by increasing the injection ratio. Since no noise sources are included in the model, high values of signal-to-intermodulation ratio at very low injection ratios are predicted. However, in current systems, these values cannot be achieved. For a fixed photo-current, the highest possible value of signal-to-intermodulation is the SNR which is determined by the noise floor of

the system. A plot of SNR as a function of average photo-current is presented in [20].Increasing the depth of phase modulation corresponds to a reduction of the signal-to-intermodulation ratio as seen in Figure 2.23 (b).

In an injection locked semiconductor laser operating at a fixed temperature, phase modulation is achieved by modulating the current of the laser. Current modulation corresponds to carrier density modulation. Due to carrier density dependence of the refractive index, the refractive index in the active region of the semiconductor laser and consequently the laser resonance frequency is modulated. Modulation of resonance frequency translates to phase modulation through Equation. In addition to phase modulation, modulation of carrier density results in amplitude modulation. This amplitude modulation can distort the output signal. The simulation results of the signal-to-intermodulation ratio of the modulator with and without residual amplitude modulation are shown in Figure 2.23 (a). Depth of phase modulation is set to 40% and depth of residual amplitude modulation to 10% of the depth of phase modulation. It can be seen that the signal-to-intermodulation ratio is degraded by ~10 dB when amplitude modulation is included in the simulation.

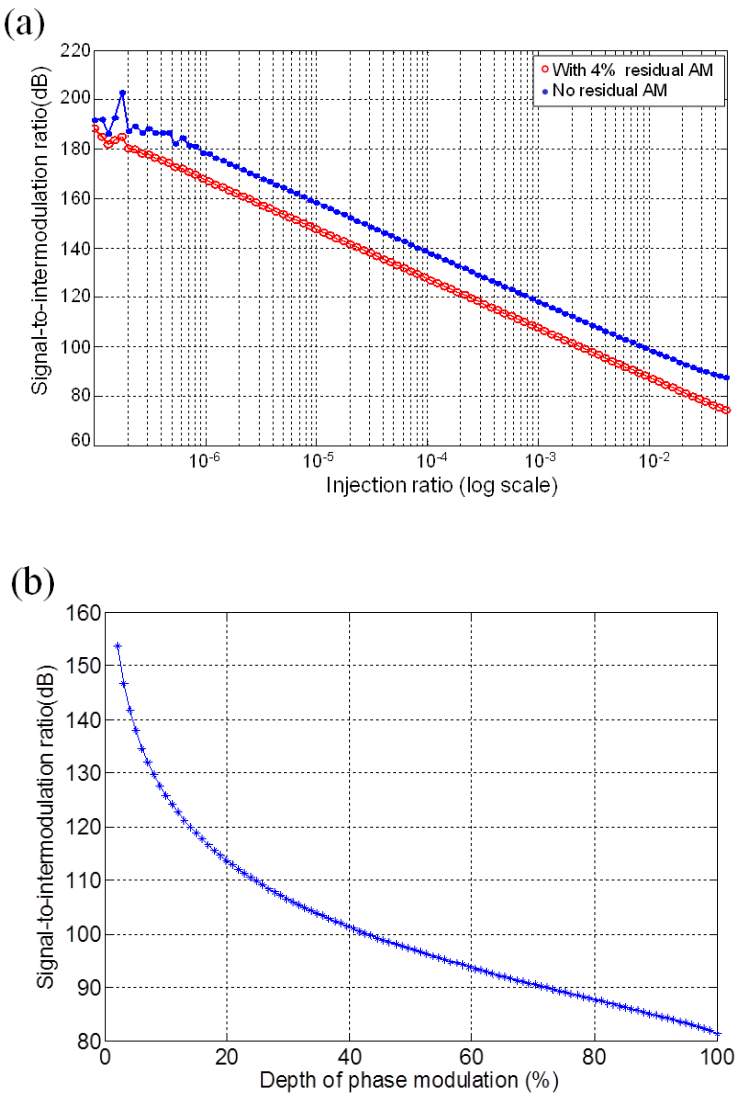

Figure 2.23. (a) Signal-to-intermodulation ratio vs. injection ratio at 40% depth of modulation, (b) Signal-to-intermodulation vs. depth of phase modulation at 0.1 injection ratio.

Finally, the nonlinear relation between refractive index and frequency (f=c/2nL where f, c, n, and L are the frequency, speed of light, refractive index and the cavity

length, respectively) introduces another limitation on the signal-to-intermodulation ratio of this modulator. Thus far in this paper, a linear frequency response for the resonant cavity is considered, i.e. current modulation is linearly related to frequency modulation. In order to observe the effect of nonlinear cavity response on the signal-to-intermodulation ratio of this modulator, two cases were considered, when the frequency modulation is obtained through modulation of refractive index using f=c/2nL (nonlinear response) and when the frequency is modulated directly (linear response). Figure. 2.24 shows the signal-to-intermodulation ratio as a function of injection ratio for these two cases at a fixed depth of phase modulation. The same depth of phase modulation is considered for both cases (40%).

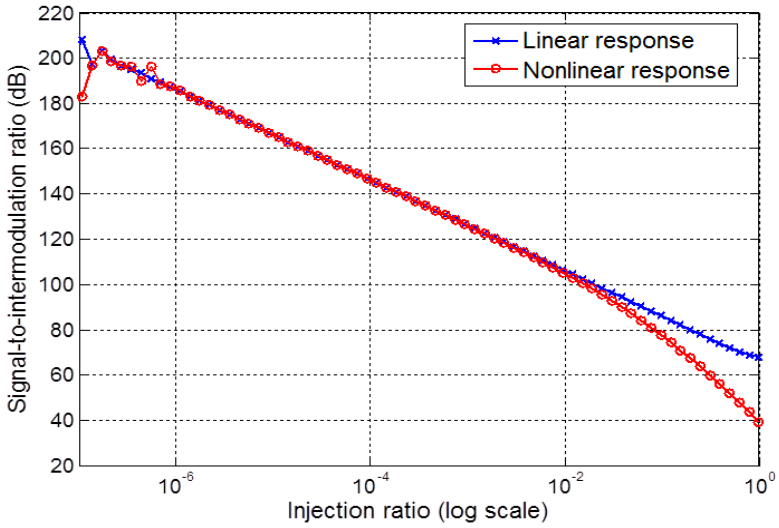

Figure. 2.24. Signal-to-intermodulation ratio vs. injection ratio for a nonlinear (red) and linear (blue) cavity responses.

As seen in Figure. 2.24, the Signal-to-intermodulation at weak injection ratios is the same for both cases. For injection ratios larger than 0.01, the separation between the linear and nonlinear cavity response is obvious. This implies that the frequency response of an injection locked semiconductor laser can be considered linear at very weak injection ratios. However, the nonlinearity of the response of the cavity has to be included in the calculation of the Signal-to-intermodulation at injection ratios higher than 0.01.

2.5 Experiments

In this section experimental results of the performance of two semiconductor resonant cavity linear interferometric modulators are presented. First modulator has a Fabry- Pérot laser as the resonant cavity with gain. In this case, injection locking happens in transmission mode. As it will be shown, due to the long cavity size (~1 mm) the depth of residual amplitude modulation is large which, as discussed in the above section, reduces the signal-to-intermodulation ratio of the modulator. The experimentally measured signal-to-intermodulation ratio is compared with the theoretically predicted values. Good agreement between the measured and theoretically predicted values of signal-to-intermodulation ratio is obtained. Second modulator setup has a vertical cavity surface emitting laser (VCSEL) as the resonant cavity with gain. Due to the small cavity size (5-6 micron), the amount of residual amplitude modulation is much smaller than the Fabry-Pérot laser. Also, lower V_π and higher bandwidth can be achieved with this setup.

2.5.1 Resonant cavity linear modulator with a Fabry-Pérot laser as the resonant cavity

The slave laser used in this experiment is a multi-mode commercially available Fabry-Pérot laser operating around 1540 nm. The Fabry-Pérot device length is ~1mm, which corresponds to 40 GHz free spectral range. A schematic of the modulator setup is shown in Figure. 2.25. The Fabry-Pérot laser is injection locked in transmission mode. If the slave laser is injection locked in reflection mode, for example in the case of injection locking a VCSEL, front facet reflection needs to be included in the simulation as well.

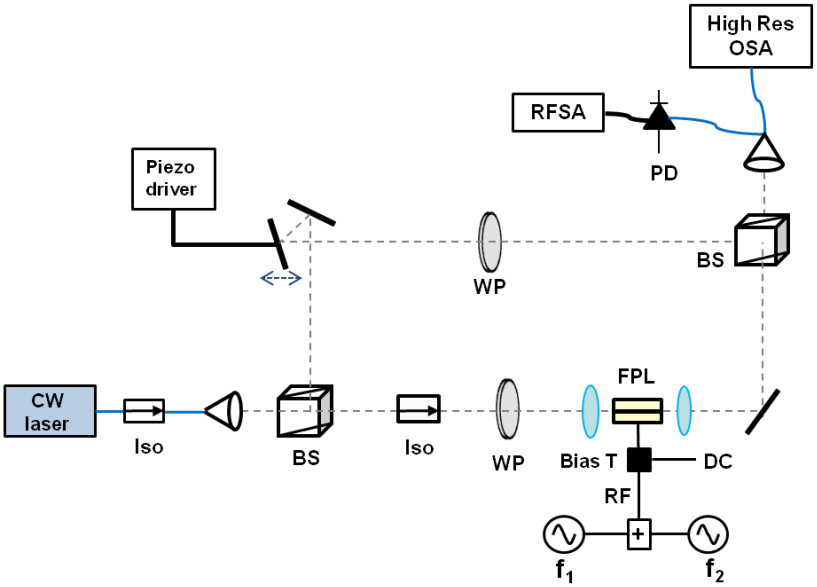

Figure. 2.25. Experimental setup for measuring the signal-to-intermodulation ratio of the modulator. BS: Beam splitter; WP: Waveplate; FPL: Fabry–Pérot laser; RFSA: Radio frequency spectrum analyzer; OSA: Optical spectrum analyzer.

In this experiment, the master laser is a commercial CW fiber laser with narrow linewidth (<2 kHz) operating at 1541.5 nm with ±0.3 nm wavelength tunability. The light from the master laser is launched into free space and split into two arms of the interferometer. Polarization of the injection light is aligned to be co-polarized with the Fabry-Pérot laser. The wavelength of the master laser is temperature tuned towards the closest Fabry-Pérot laser mode. When the injection seed is within the locking range, the slave Fabry-Pérot laser locks to the master laser. The optical spectrum of the Fabry-Pérot laser before and after injection locking is shown in Figure. 2.26. Other modes of the Fabry-Pérot laser are suppressed by ~ 44 dB.

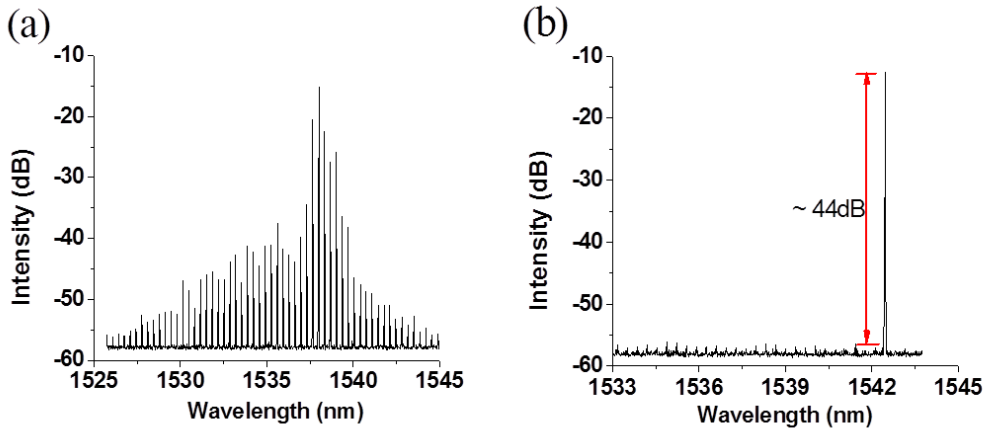

Figure. 2.26. Optical spectra of the Fabry-Pérot laser (a) not injection locked (b) injection locked.

As it mentioned in the previous section, the undamped relaxation oscillations of an injection-locked semiconductor laser can cause instability and as a result reduction of the stable locking range. The damping factor is higher for negative detuning than positive

detuning frequencies. We studied the evolution of the undamped relaxation oscillation tones within the locking range of the injection locked Fabry-Pérot laser. The optical spectrum at the output of the injection-locked laser is observed when the driving current of the Fabry-Pérot laser is increased from 57 mA to 67.8 mA (the most negative detuning point towards the zero detuning) which, corresponds to a locking range of 2.65 GHz, see Figure 2.27 (a)-(d). As seen in this figure, the relaxation oscillations are damped at the most negative detuning frequency. As the drive current increases, the relaxation oscillation tones at 3.6 GHz away from the carrier are starting to come up and they get stronger as the current increases (towards positive detuning). Finally, the undamped relaxation oscillations cause the laser to enter an unstable region. Note that the tones observed at 4 GHz away from the carrier are the high resolution optical spectrum analyzer artifacts used in these experiments.

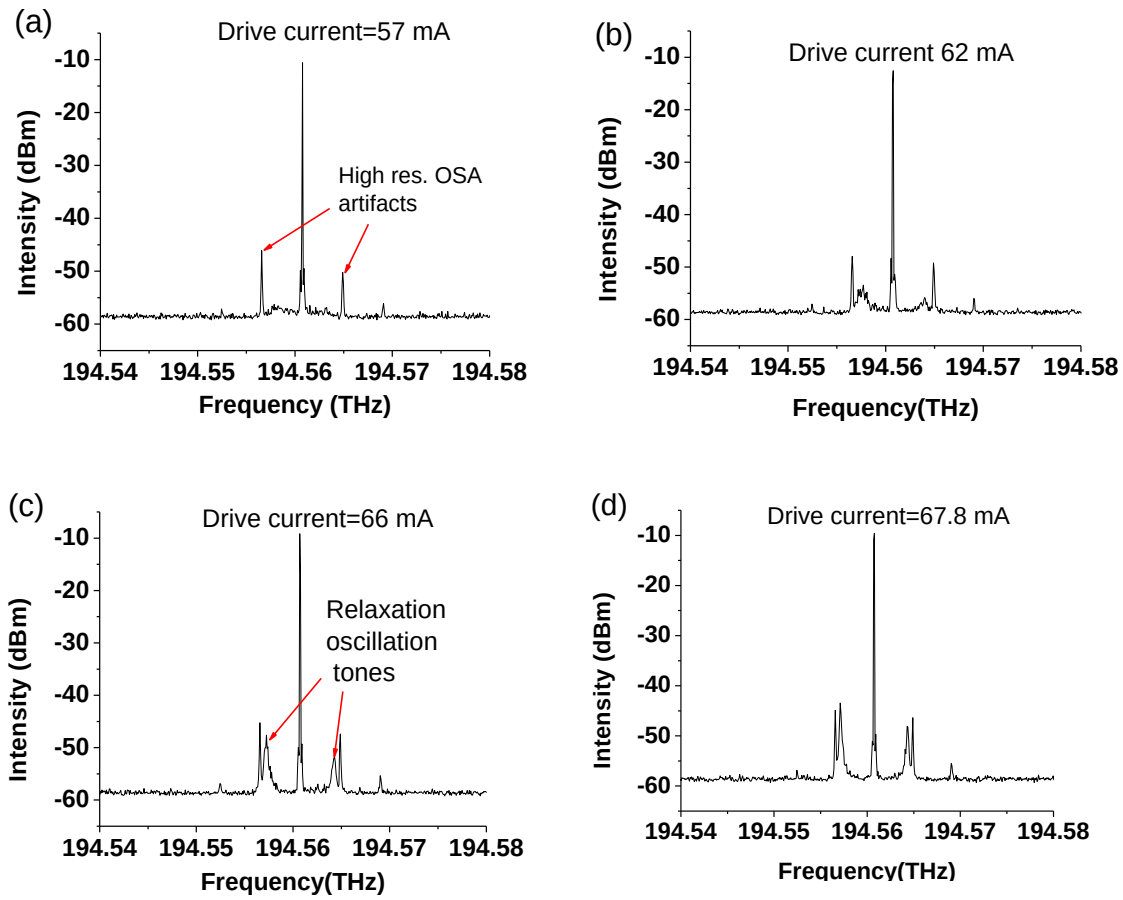

Figure 2.27. (a)-(d)Evolution of the undamped relaxation oscillation frequencies within the locking range.

After injection locking the Fabry-Perot laser, the output light from the injection locked slave laser is then combined with the reference arm of the interferometer in quadrature. Polarization and the optical powers of the two arms of the interferometer are matched to achieve the maximum depth of modulation of the output intensity modulated light. To measure the signal-to-intermodulation ratio of this modulator, the driving

current of the slave laser is modulated at 300 and 400 MHz simultaneously. The detected output signal is split in two equal parts and sent to two radio frequency spectrum analyzers (RFSA). One RFSA is used to monitor the fundamental frequencies and the other to monitor the third order intermodulation tones with high resolution. The signal-to-intermodulation ratio at various RF drive power is measured. Signal-to-intermodulation ratio is the ratio of the detected fundamental frequency tone power to the third-order intermodulation tone power. Sample RF spectra are shown in Figure 2.28 (a) and (b) Figure 2.28 (a) shows the fundamental frequencies at f_1=300 and f_2=400 MHz when the modulator is driven at -25 dBm. Figure 2.28 (b) and (c) show the RF spectra measured with higher resolution (RBW 100 Hz) centered at the third-order intermodulation frequency $2f_1$-f_2=200 MHz. From these graphs the signal-to-intermodulation ratio can be calculated to be ~50 dB.

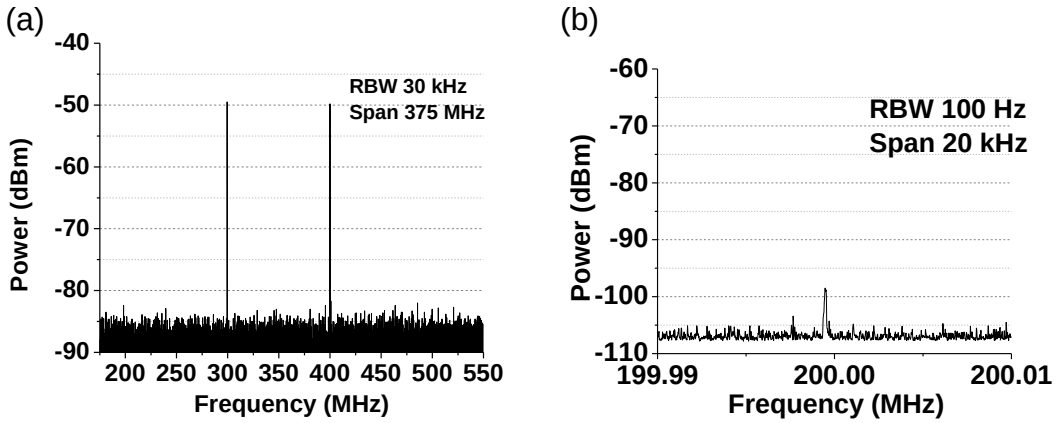

Figure 2.28. Detected RF power spectra (a) fundamental frequencies (b) one of the third-order intermodulation frequencies (200 MHz).

To compare the experimental results with the theoretical predictions, the measured depth of amplitude modulation and frequency detuning were used in the simulation. The injection ratio was fixed to 0.1 for all the measurements. The locking range was measured to be 2.95 GHz. The alpha parameter and the impedance of the diode laser were assumed to be 2 and 12 ohm, respectively. The measured and theoretical values for signal-to-intermodulation ratio are plotted in Figure 2.29.

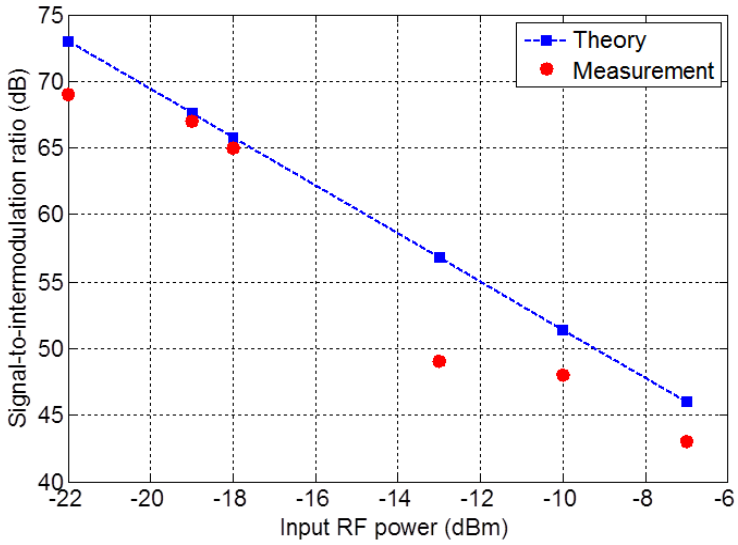

Figure 2.29. Theoretically calculated and measured values of signal-to-intermodulation ratio at different input RF drive powers with 0.1 injection ratio.

2.5.2 Resonant cavity linear modulator with a VCSEL as the resonant cavity

The semiconductor laser used in this section is a commercially available single mode vertical cavity surface emitting laser (VCSEL). VCSELs are semiconductor lasers with the active layer sandwiched between two highly reflective dubbed distributed Bragg

reflectors (DBRs). DBR mirrors are made up of several alternating high and low refractive index quarter-wavelength thick layers of semiconductors. Figure 2.30 shows the structure of a VCSEL.

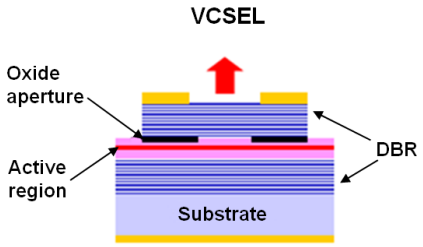

Figure 2.30. Structure of a VCSEL device.

The VCSEL device used in these experiments is a single mode, fiberized device operating at ~1550 nm (C-band). Device length is ~ 5-6 μm. The L-I curve (output power vs. drive current) is shown in Figure 2.31 (a). This device has a threshold of ~ 2mA and a maximum output power of 1.025 mW.

By tuning the drive current of the VCSEL the output frequency can be changed. The plot of output frequency vs. drive current is shown in Figure 2.31 (b).The tunability of this VCSEL is ~56.86 GHz/mA.

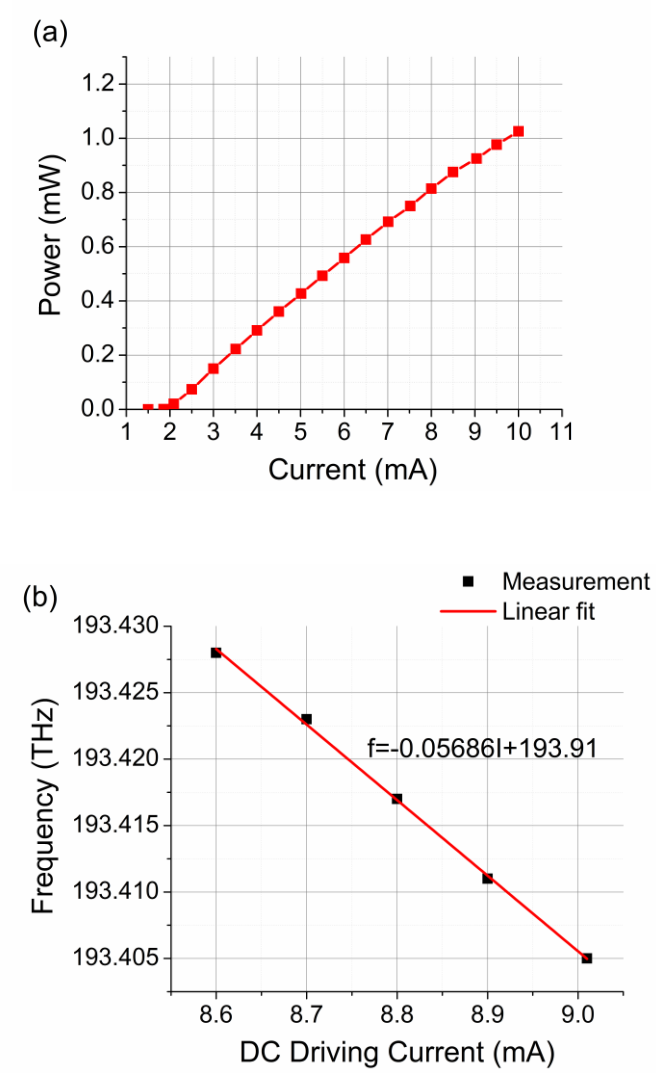

Figure 2.31. Characteristics of the VCSEL device used in the experiment (a) L-I curve (b) frequency tunablity curve.

A schematic of the linear modulator implemented with the VCSEL and commercially fiberized components is shown in Figure 2.32. The CW laser used for injection has high frequency stability and narrow linewidth (<1 kHz) for stable injection

locking (Orbits ligthwave). A variable optical attenuator controls the amount of optical power injected into the VCSEL since the ratio of this power to the output power of the VCSEL directly related to the locking range. Phase modulation is achieved by modulating the driving current of the VCSEL. Current modulation results in a modulation of the carrier density, follows by index of refraction modulation which corresponds to modulation of frequency of the cavity resonance through f=c/2nL. An optical phase shifter is used to set the two arms of the interferometer in quadrature, which is necessary for the linear response of the modulator. It should be noted that in this configuration, an overall optical gain of the signal can be realized.

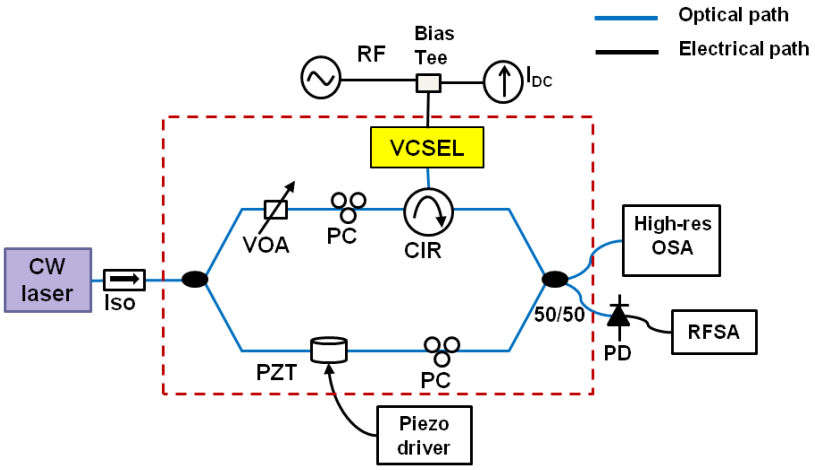

Figure 2.32. System diagram: VCSEL: Vertical cavity surface emitting laser, VOA: Variable optical attenuator, PZT: Piezo electric transducer, PC: Polarization controller, Iso: Isolator, CIR: Circulator, PD: Photodetector, RFSA: Radio frequency spectrum analyzer, High-res OSA: High resolution optical spectrum analyzer.

In order to measure the induced static phase shift of the injection-locked VCSEL for a certain injection seed power, the resonant frequency of the VCSEL was tuned within the locking range by varying the bias current of the VCSEL. The corresponding induced phase shift was obtained from the DC voltage of the detected signal and an arcsine function was fit to it, as shown in Figure 2.33. The VCSEL bias current deviation of ~52 μA resulted in a total phase shift of 0.7π. From the arcsine fit, the required current deviation for a π phase shift was estimated. Knowing the impedance of the VCSEL device, the effective V_π of the modulator was calculated to be ~2.6 mV. The stable locking range measured to be ~ 5 GHz.

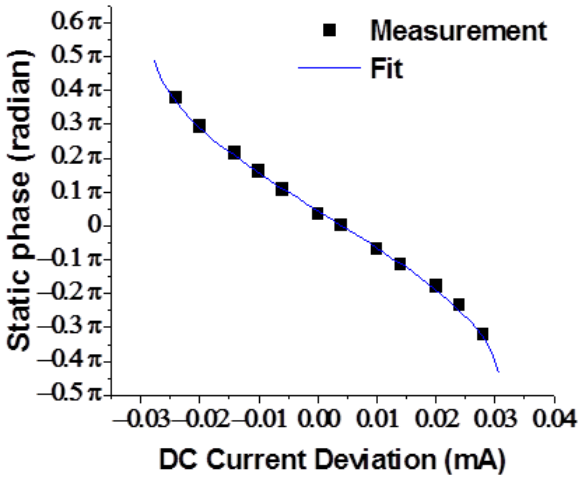

Figure 2.33.Static phase shift plot of the injection-locked VCSEL.

The modulator output along with the small AC-signal response of the modulator is shown in Figure 2.34 (a) and (b). The modulator shows an intensity modulated output

signal with 40% depth of modulation, driven by a 20 MHz sine wave, Figure 2.34 (a). The small AC-signal response of the modulator is shown in Figure 2.34 (b). The -10 dB bandwidth was measured to be 5 GHz limited by the frequency response of the commercial VCSEL used in this experiment. It is anticipated that frequency response approaching 20 GHz is possible. At low frequencies, in addition to carrier modulation, modulation of the cavity length due to thermal effects contributes to the total phase modulation. However this effect reduces by increasing the frequency which corresponds to a low frequency roll-off in the frequency response curve.

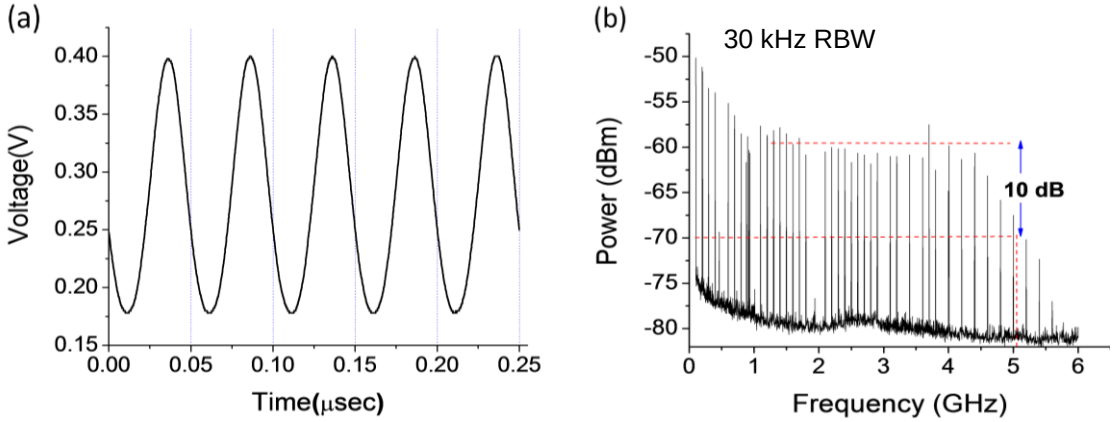

Figure 2.34. (a) Detected intensity modulated signal at the output of the resonant cavity modulator at 20 MHz modulation frequency and (b) frequency response of the linear modulator. The -10 dB bandwidth is ~5 GHz.

A two-tone intermodulation experiment was performed to measure the dynamic range of the modulator. Fundamental frequencies were chosen to be at 300 MHz and 400

MHz. Response of the system to the fundamental frequencies and their third-order intermodulation components (200 and 500 MHz) was studied. Low resolution RF power spectrum of the system (1 MHz RBW), Figure 2.35(a), shows no intermodulation tones. Figure 2.35 (b) is the RF power spectrum around the 500 MHz intermodulation component obtained with high resolution (1 Hz RWB). The resulting dynamic range is 95 dB, which is limited by the noise floor and instability of the fiberized system. The latter is due to fluctuations in fiber length from environmental factors, which corresponds to deviation of the differential phase from quadrature.

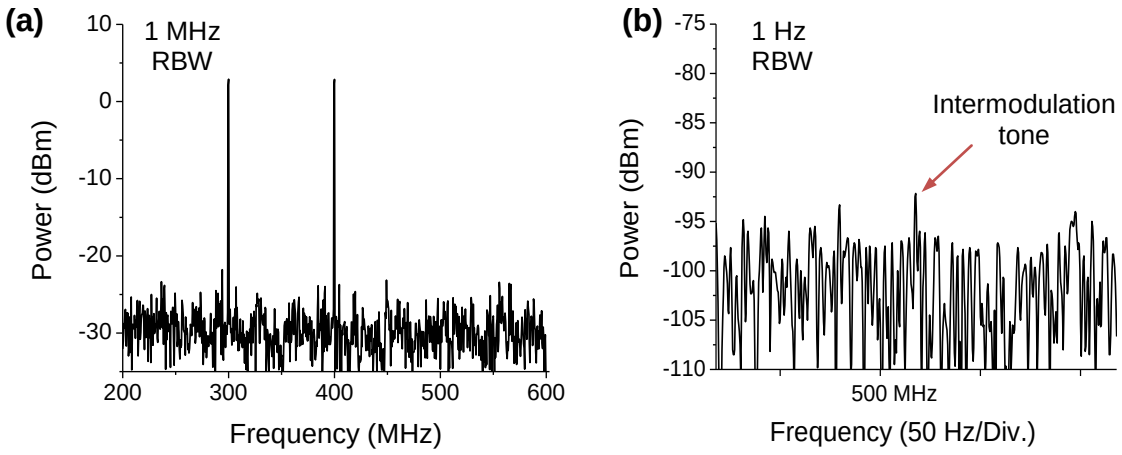

Figure 2.35. SFDR measurements: (a) Power spectrum at the output of the two-tone SFDR measurement using 300 and 400 MHz tones (b) Low resolution bandwidth (1 Hz) spectrum of the 500 MHz third order intermodulation tone.

The measured frequency change of the VCSEL versus temperature is 15 GHz/^{o}C. Given the locking range of 5 GHz, implies that a temperature stability of ~0.3 ^{o}C is

required in order to use the injection locked VCSEL as a phase modulator. This requirement can be easily achieved by using a commercial TEC giving 0.02 ^{o}C stability.

The frequency stability of the VCSEL before and after injection locking is studied which can explain the rise of the noise floor in the two-tone measurement of this modulator. Figure 2.36 shows the experimental setup for this measurement. The light from VCSEL beats with a stable CW source whose frequency is 3.687 GHz away from the VCSEL frequency. The resultant heterodyne beat is observed on a real time RFSA. Figure 2.37 is the spectrogram of the beat note when the VCSEL is free running. As seen in this figure, the free running VCSEL frequency fluctuates within a 2 GHz span. The fluctuations in the frequency are predicted to be from the fluctuation in the drive current of the VCSEL. However, when the VCSEL is injection-locked to a stable master laser, the VCSEL (slave laser) follows the master laser frequency which results in a more stable output from injection-locked VCSEL in compare to the free running case. The increase in the frequency stability of the VCSEL by injection locking can be clearly seen in Figure 2.38.

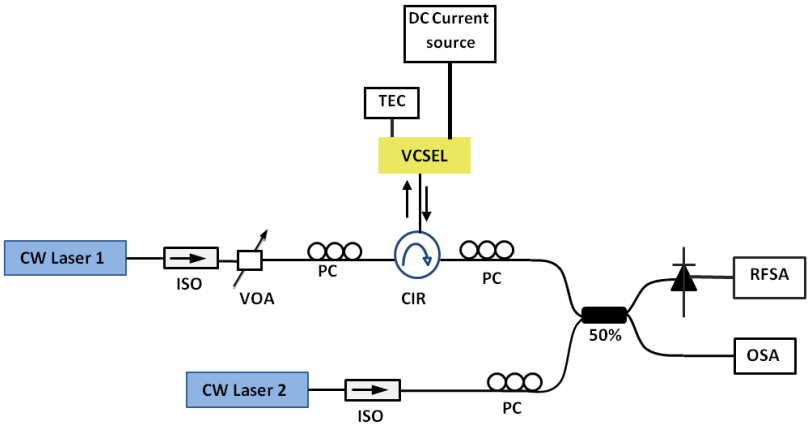

Figure 2.36. Frequency stability measurement setup.

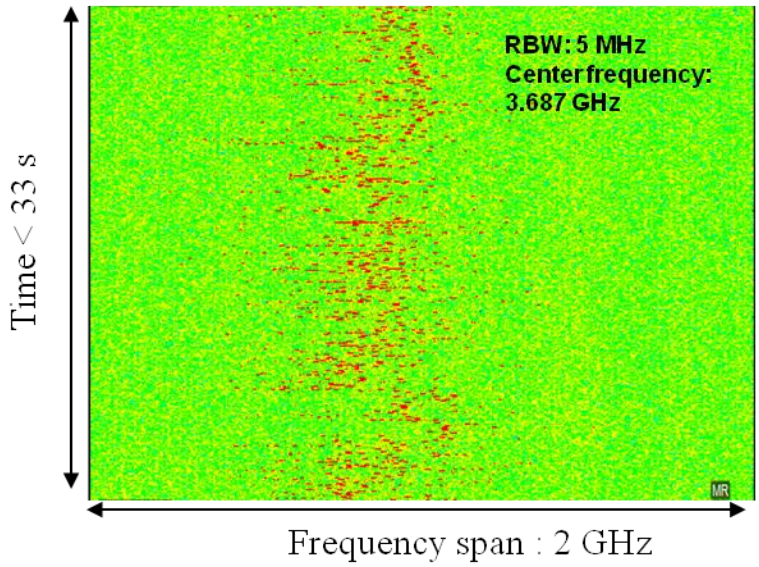

Figure 2.37. Free running VCSEL beating with a stable source (Orbits lightwave).

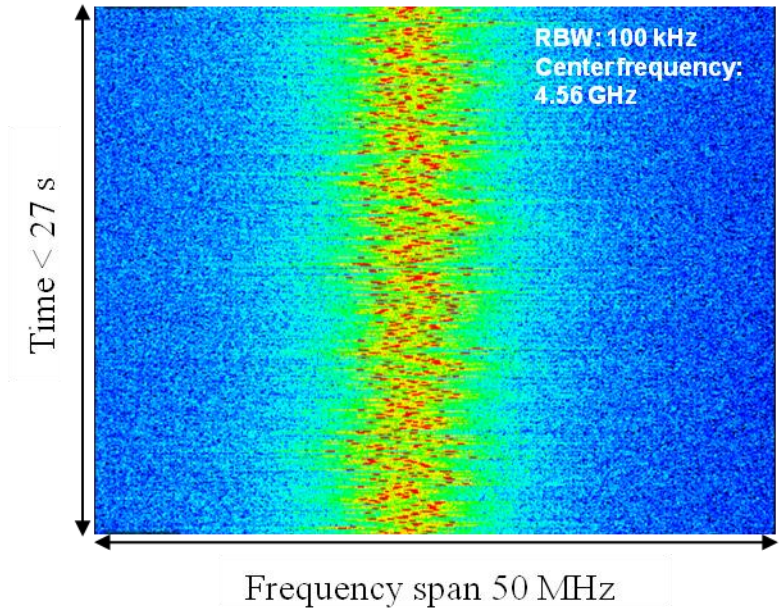

Figure 2.38. Injection-locked VCSEL beating with a stable source (Orbits lightwave).

When the VCSEL is injection-locked, the frequency fluctuations of the VCSEL observed in Figure 2.37 are converted to phase noise which causes an increase in the noise floor of the detected signal. The phase noise added by the injection-locked VCSEL can limit the maximum achievable SFDR of the linear modulator with VCSEL as the resonant cavity. Chapter 4 of this thesis is on the study of the phase noise added by an injection-locked VCSEL. A self-heterodyning beat between the injection-locked VCSEL and the frequency shifted master laser is measured for the study of the phase noise added by the injection-locked VCSEL.

2.5.3 Measurements of the linear modulator SFDR

To measure the SFDR of the linear modulator, two-tone experiment should be performed at several RF input powers. Since the modulator setup shown in Figure 2.32 is constructed with all fiberized components, the fluctuations in the fiber length results in a slow drift of the bias point from the quadrature during the experiment. In order to measure the maximum SFDR of this modulator, the bias point of the modulator should be locked at quadrature.

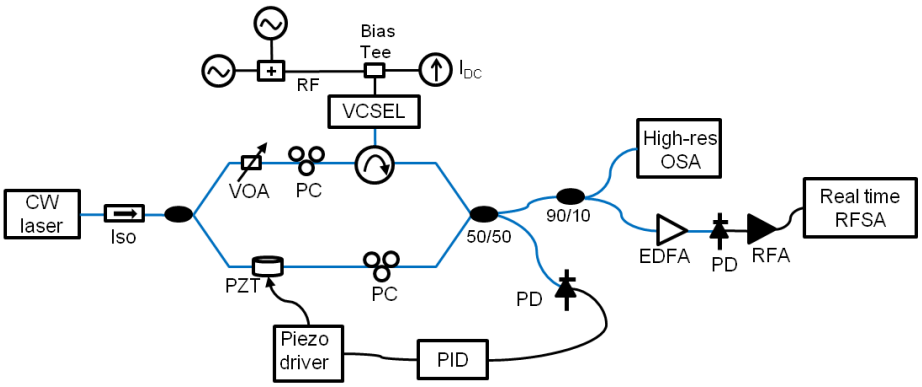

Figure 2.39. System diagram of the linear modulator with a simple bias point locking scheme. Iso: Isolator; VOA: Variable optical attenuator; PC: Polarization controller; VCSEL: Vertical cavity surface emitting laser; PZT: piezoelectric transducer (fiber stretcher); EDFA: Erbium-doped fiber amplifier; PD: Photodetector; OSA: Optical spectrum analyzer, PID: proportional-integral-differential controller; RFA: Radio frequency amplifier; RFSA: Radio frequency spectrum analyzer.

To do so, a simple locking scheme was used to lock the modulator bias point, see Figure 2.39. The locking scheme is based on detection of slow drift in the optical power which is due to the fiber length fluctuation. As it can be seen in Figure 2.39, half of the modulator output is photodetected and sent to a proportional-integrated-differential (PID) controller. Since the PID controller has a bandwidth of a few kHz, only the change in the optical power which is due to the slow fluctuations of the path length in the fiberized interferometer are seen by the PID controller which sends the correction signal to the piezo controller. The bias point of the modulator can be set using the adjustments on the

PID controller. Also it should be mentioned that to minimize the fiber length fluctuations, the modulator is placed in box with thermal and acoustic insulation. Error signal with locking off and on over a period of 10 seconds is shown in Figure 2.40.

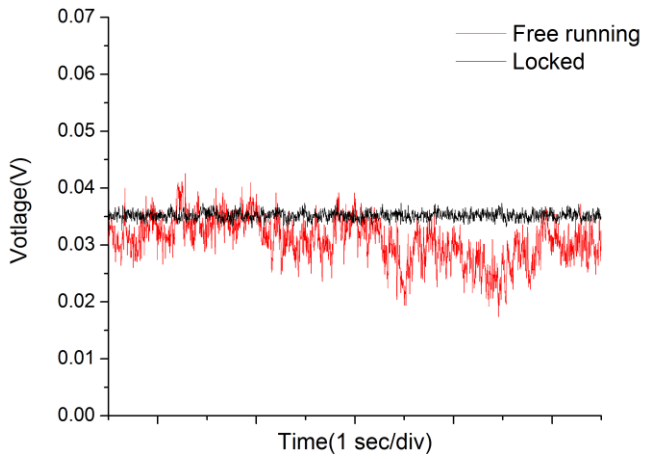

Figure 2.40. Error signal before and after locking the bias point of the modulator taken over 10 second.

The driving current of the VCSEL is modulated simultaneously at two different RF frequencies (1 and 1.001 GHz) but equal powers. Photodetected spectrum of the modulator was measured for -27,-30,-33 and -36 dBm of input RF power. Figure 2.41 shows a sample of photodetected spectrum at input RF power of -36 dBm directly from the modulator. Both fundamental (1 and 1.001 GHz) and third-order intermodulation (0.999 and 1.002 GHz) tones can be observed at this input RF power.

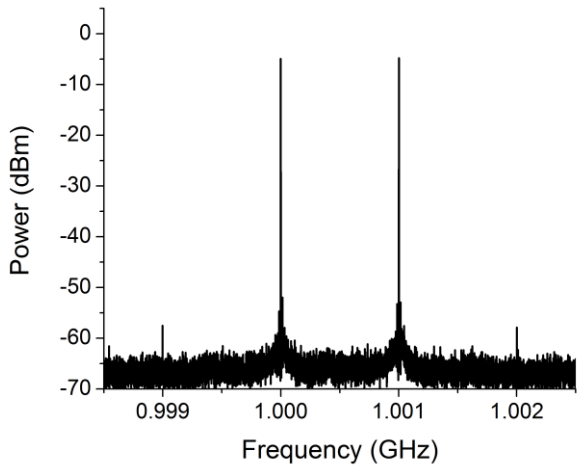

Figure 2.41. Sample photodetected RF spectrum of the modulator at -36 dBm input RF power.

The results of the two-tone measurements are summarized in a plot of fundamental and third-order intermodulation product power as a function of modulator input RF power, see Figure 2.42. As it was expected, linear fits of the data have slope of 1 and 3 for fundamental and third-order intermodulation, respectively.

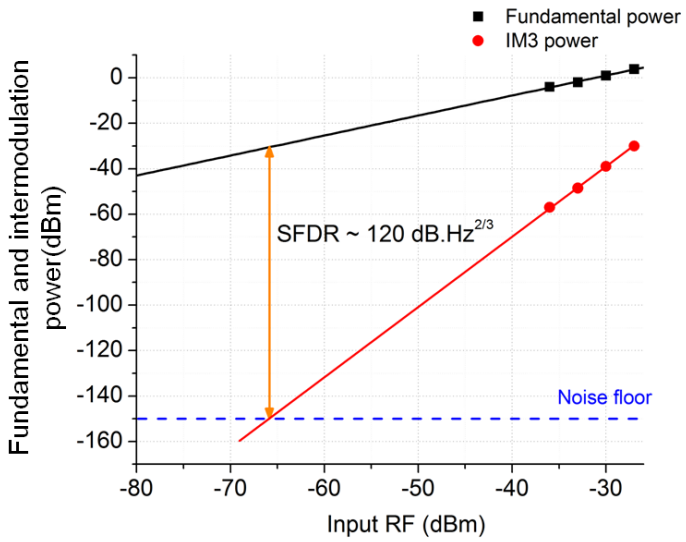

Figure 2.42. Fundamental and third-order intermodulation power vs. input RF power to the modulator.

To calculate the SFDR of this modulator from the plot in Figure 2.42, the noise floor of the system should be determined. The RIN-limited noise floor of the system is measured and compared with the thermal noise and shot noise-limited values. Figure 2.43 shows the measured RIN of the free running VCSEL, injection seed laser and injection-locked VCSEL. It is interesting to note that the high relaxation oscillation peak at ~0.6 MHz frequency seen in the RIN plot of the seed laser has been attenuated by ~40 dB after injection locking the VCSEL. Moreover, at low offset frequencies reduction of the VCSEL RIN after injection locking is observed. However, at high offset frequencies (>100 MHz) the RIN of the injection-locked VCSEL overlaps with the RIN of the free running VCSEL.

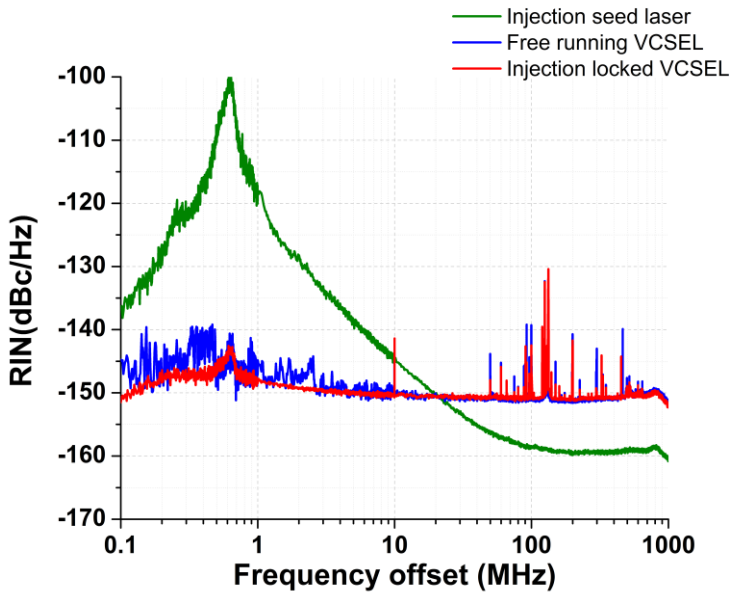

Figure 2.43. Measured RIN of the injection seed laser, free running VCSEL and injection locked VCSEL at 5.95 mA.

The average optical power on the detector is ~ 8 mW. Using this value and knowing the responsively of the photodetector (0.8 A/W), the thermal and shot noise floor of the system calculated to be -174 and -160 dBm/Hz. From calculated values of the shot noise and thermal noise of the system, we determined that the system is RIN-limited. The RIN of the injection-locked VCSEL at offset frequencies around 1 GHz is -150 dBc/Hz. By using this value for the noise floor of the system, the SFDR from the modulator was calculated to be 120 dB. $Hz^{2/3}$.

As it is shown in Figure 2.14, numerical simulation predicts a high dependency of the SFDR of a resonant cavity interferometric modulator to the modulator bias point. To experimentally investigate this dependency, SFDR was measured at the output of the

modulator at different bias points. Figure 2.44 summarizes the results. It can be seen that the SFDR of this modulator is the highest at quadrature which is in agreement with the theoretical prediction in Figure 2.14.

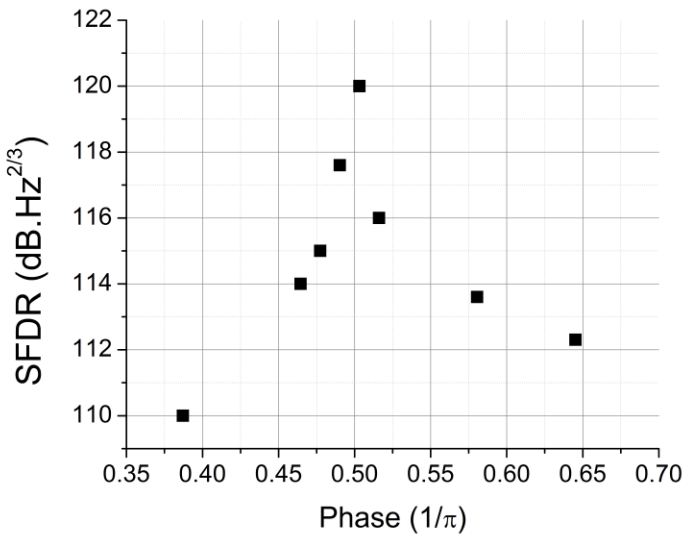

Figure 2.44. Measured SFDR directly after the modulator vs. bias point of the modulator.

2.5.4 SFDR measurements of an analog optical link with the linear modulator

A schematic of the experimental setup of the analog link using a resonant cavity interferometric modulator is shown in Figure 2.45. On the transmitter side, the light from a CW fiber laser at 1550 nm is sent to the modulator. All fiberized and commercially available components in the C-band are used in this setup. The resonant cavity of the modulator is a temperature-controlled VCSEL operating at ~1550 nm with 5 nm tunablity. A CW laser injection locks the VCSEL operating in reflection mode.

An injection power on the order of 1 μW was used in all of the experiments. Considering the output power of the VCSEL (~0.6 mW at 5.95 mA bias current), this injection ratio (~-27 dB) corresponds to operating in the weak injection regime of the modulator. At this injection ratio, the locking range of the VCSEL is measured to be ~3 GHz. The weak injection regime is the preferred mode of operation for the modulator for several reasons. First, for weak injection, nearly the entire locking range is within the stable locking range and a larger depth of phase modulation can be achieved. Secondly, weak injection results in a small frequency locking range that translates to a low RF drive power to achieve arcsine phase modulation. And finally, owing to the low RF drive power, a small unwanted amplitude modulation is generated due to the small change of carrier density. By modulating the current of the injection-locked VCSEL, the VCSEL's free running cavity frequency is modulated, resulting in arcsine phase modulation. The phase modulated light from the injection-locked VCSEL is combined with the reference arm in a 3-dB fiber coupler. The same locking scheme as the previous section is used here. One of the outputs of the interferometer is photodetected and sent to a PID controller. Since the PID controller has a bandwidth of a 100 kHz, only changes in the optical power corresponding to the slow fluctuations of the path length in the fiberized interferometer are compensated by it. The PID controller sends the correction signal to the piezo controller to adjust the path length and hence to keep the modulator biased at a fixed point. The bias point of the modulator is set by adjusting the setpoint on the PID controller.

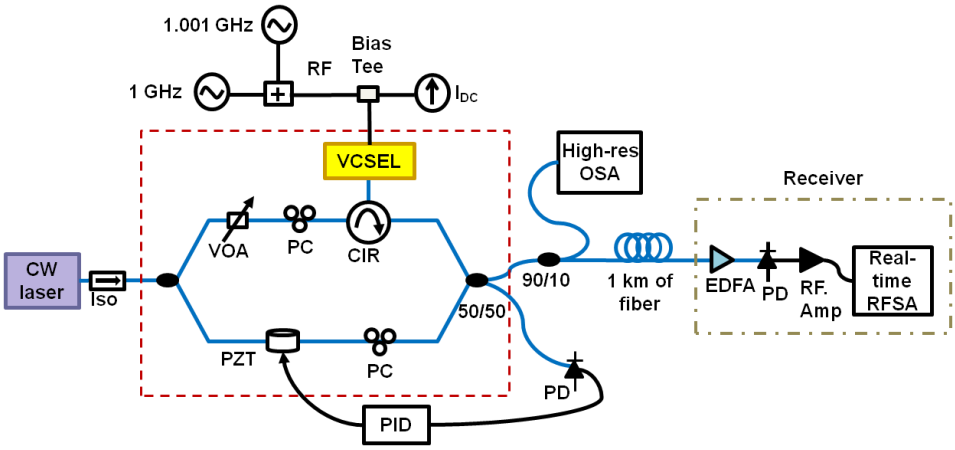

Figure 2.45. System diagram of an analog optical link with a linear modulator. Iso: Isolator; VOA: Variable optical attenuator; PC: Polarization controller; VCSEL: Vertical cavity surface emitting laser; PZT: piezoelectric transducer (fiber stretcher); EDFA: Erbium-doped fiber amplifier; PD: Photodetector; High-res OSA: High resolution optical spectrum analyzer, PID: proportional-integral-differential controller; RFA: Radio frequency amplifier; RFSA: Radio frequency spectrum analyzer.

An analog link employing this modulator was constructed using 1 km SMF. In order to measure the SFDR of this link, two-tone experiments were performed at different RF input powers. The modulator's bias point is locked as close as possible to quadrature. For each input RF power, the driving current of the VCSEL is modulated simultaneously at two different RF frequencies (1 and 1.001 GHz) of equal powers. The output signal is sent over 1 km of SMF and optically amplified to 8 mW at the receiver side using an EDFA. The photodetected RF power spectrum of the modulator was measured for drive powers of -23,-26,-29 and -32 dBm input RF power. Figure 2.46 shows a sample of the

photodetected spectrum at an input RF power of -29 dBm. Both fundamental (1 and 1.001 GHz) and third-order intermodulation (0.999 and 1.002 GHz) tones can be observed at this input RF power. The results of these measurements are summarized in a plot of power in the fundamental and third-order intermodulation tones as a function of modulator input RF power, see Figure 2.47. To calculate the SFDR of this modulator from the plot in Figure 2.47, the noise floor of the system should be determined. The RIN of the free running VCSEL, injection seed laser and injection-locked VCSEL were measured. Again here, the noise floor of the system determined to be RIN-limited. Using the RIN-limited value for the noise floor of the system, the SFDR of the link is calculated to be 120 dB.Hz$^{2/3}$.

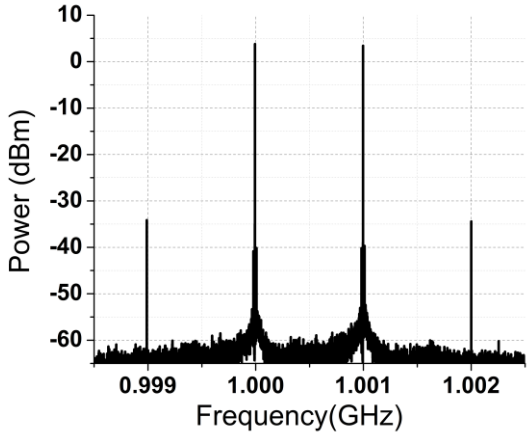

Figure 2.46. Sample photodetected RF spectrum at the receiver side.

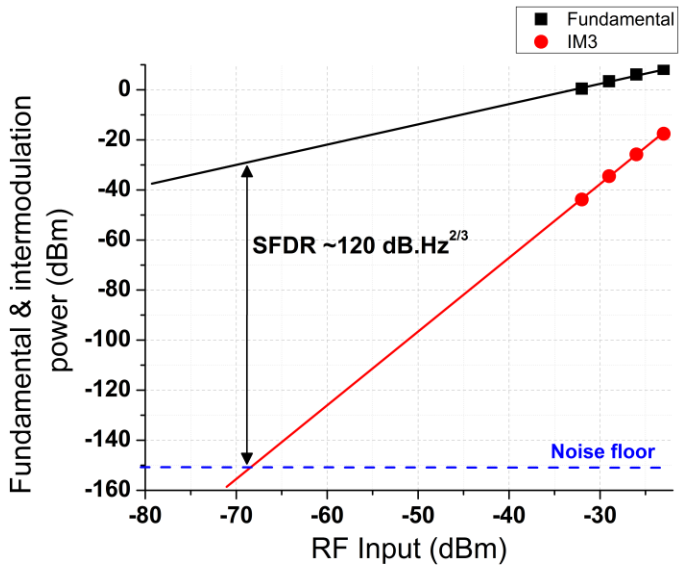

Figure 2.47. Fundamental and third-order intermodulation power vs. input RF power to the modulator. The analog link SFDR is calculated to be 120 dB.Hz$^{2/3}$.

As it is seen in Figure 2.43 the RIN of the injection-locked VCSEL is 10 dB higher than the RIN of the injection seed at offset frequencies around 1GHz. This implies that the SFDR of the system can be improved by at least 10 dB by canceling the common mode noise. Common mode noise cancellation can be achieved by balanced photodetection [53] or a delayed differential RIN cancellation [54] at the receiver side. In addition to lowering the system noise floor from -150 dBc/Hz to -160 dBc/Hz, these detection techniques generate higher photo current compare to direct detection which can further improve the SFDR. Hence, SFDRs in the order of 130 dB.Hz$^{2/3}$ or higher are expected for this modulator.

2.6 Discussions and conclusion

In this Chapter, we introduced a novel, simple, efficient linear modulator. This interferometric modulator has an injection locked laser as an arcsine phase modulator.

Our theoretical study of the linearity of the interferometric linear intensity modulator with a semiconductor laser as the resonant cavity shows the dependence of the SFDR of such a modulator on alpha parameter, injection ratio, residual amplitude modulation, depth of modulation and the linearity of the cavity frequency response.

A non-zero alpha parameter of the injection locked semiconductor laser results in an asymmetric locking range so that the maximum achievable phase shift is from $\cot^{-1}\alpha$ to $-\pi/2$. Also above a certain level of injection ratio, undamped relaxation oscillations further limit the stable locking range and as a result, the range of achievable phase shifts. In the laser cavity used in the simulation, the regions of instability are observed for injection ratios above -14 dB. The asymmetric phase response of the injection locked semiconductor laser degrades the SFDR of the modulator. In order to reduce the effect of a non-zero alpha parameter, the lasing frequency of the slave semiconductor laser can be shifted by tuning the operating temperature, to the peak of the gain spectrum. At this operating point, the alpha parameter is close to zero.

The weak injection regime can be considered the ideal operating regime for this modulator. At low injection ratios, the residual amplitude modulation can be reduced without sacrificing the depth of phase modulation. Weak injection corresponds to a narrow locking range. Consequently, a small frequency detuning is required to achieve phase modulation. The smaller the frequency detuning range, the smaller the required

carrier density change to span the entire range, leading to lower residual amplitude modulation. Moreover, in weak injection regimes, the cavity frequency response of the injection locked semiconductor laser can be considered to be linear. For the semiconductor laser used in the simulation (Table 1), injection ratios less than -20 dB corresponds to a maximum achievable phase shift ($\cot^{-1}\alpha=0.1024\pi$ to $-\pi/2$), linear cavity frequency response and small residual amplitude modulation.

In conclusion, a theoretical study of the SFDR of a semiconductor resonant cavity linear interferometric intensity modulator is presented in this paper. Starting from the rate equations describing an injection locked semiconductor laser, the output power of the injection locked laser and the phase response across the locking range were obtained. It is shown that for a non-zero alpha parameter, the locking range is asymmetric. Effects of injection ratio, alpha parameter, residual amplitude modulation, depth of phase modulation, and linearity of cavity response on the SFDR of the modulator were studied. The highest SFDR can be achieved for low injection ratios and small depth of phase modulation where the instability region of the locking range and residual amplitude modulation are both minimal.

Experimental results of the SFDR measurements of a modulator with a Fabry-Pérot laser, injection locked in transmission, were compared to the theoretically predicted values. Good agreement between the calculated and measured values of SFDR is obtained.

Finally, we present the experimental results of the linear modulator with a VCSEL device as the resonant cavity. Using commercially available fiberized

components, we obtained a V_π of ~ 2.6 mV, a -10 dB bandwidth of 5 GHz and 95 dB dynamic range. We have shown that by locking the bias point of the modulator, high SFDR can be achieved. SFDR of 120 dB.Hz$^{2/3}$ is shown for an optical analog link employing this modulator. This is limited by the RIN of the injection locked VCSEL which is 10 dB higher that the injection seed laser. Higher SFDR is predicted for this modulator by using a balanced photodetector or differential RIN cancellation for cancelling the common mode noise. In addition to lowering the system noise floor these detection techniques generate higher photo current compare to direct detection which can further improve the SFDR. Hence, SFDRs in the order of 130 dB.Hz$^{2/3}$ or higher are expected for this modulator.

CHAPTER 3: DIRECT DEMODULATION AND CHANNEL FILTERING OF PHASE MODULATED OPTICAL SIGNALS

3.1 Introduction

In this Chapter, the first experimental results of detecting phase modulated optical signals using an injection locked semiconductor laser (here VCSEL) under forward-bias condition are presented. Detection of phase modulated optical signals using an injection locked semiconductor laser was first predicted by Lidoyne and Gallion in [55]. It has been shown theoretically that a semiconductor laser locked to a phase modulated optical signal can convert the phase modulation into voltage modulation. The modulation of voltage is due to the change of carrier density in the active region of the locked diode laser when it is driven by an external phase modulated signal. It should be noted that this mechanism is the reverse of the phase modulation functionality described in Chapter 2. Channel selection capability of an injection locked tunable semiconductor laser has been demonstrated in [56]. In this Chapter, channel selection of an injection locked VCSEL in combination with detection of phase modulated optical signals will be demonstrated.

3.2 Theory

The demodulation functionality can be realized by relying on the reversible nature of an injection locked resonant cavity. For example, consider the injection locked VCSEL, one can realize filtering and direct detection of pure phase modulated analog signals using the same device. An analog phase modulated light signal is a frequency modulated signal, since the instantaneous frequency is defined as the temporal derivative

of the time varying phase modulated signal. As a result, the input to the injection locked semiconductor laser is an optical frequency that is shifting with respect to the natural resonant lasing frequency of the semiconductor laser. As the semiconductor laser is injection locked, with a given dc bias current, the injection locked semiconductor laser locks to the input instantaneous frequency of the phase modulated signal. Since the semiconductor laser is now locked to the new input frequency the cavity length must change to allow this to happen. From Chapter 2 we know that the injection current causes the cavity length and natural resonant frequency to change. In the current situation, since the dc current is not varying, but the output injection locked frequency does, the refractive index of the gain medium, hence, the carrier concentration must change to accommodate the cavity length change. Since the carrier concentration changes, there must be an accompanying change in the voltage drop across the semiconductor laser. It is this change in the voltage across the semiconductor laser that detects the instantaneous frequency, or time varying phase modulated signal, see Figure 3.1.

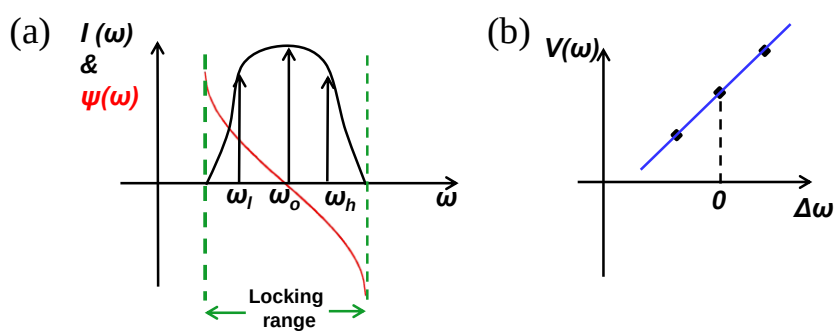

Figure 3.1. (a) Phase and amplitude response within the locking range, (b) Change of the voltage across the active region of the injection locked semiconductor laser by changing the master laser frequency in time.

As seen in Figure 3.1, if the instantaneous frequency of the injection light changes in time within the locking range, the voltage increases at positive and decrease from the value at zero detuning at negative detuning. This can be explained as follow: when the injected frequency is negatively detuned with respect to the semiconductor laser's natural resonant oscillating frequency, then the semiconductor laser output frequency shifts to lower frequency, equal to the injection frequency. Since the output frequency is lowered, the cavity length must increase, and hence the refractive index of the gain region must have increased. The increase in refractive index must be induced by a reduction of the carrier concentration and hence a drop in the voltage across the semiconductor laser. This inverse relation between the carrier concentration and refractive index in semiconductor lasers is well known and is called 'the plasma effect'[57]. Similarly, an injection frequency which is positively detuned induces a shorting of the laser cavity, hence a reduction of the refractive index, and an increase in the carrier concentration and an increase in the voltage across the semiconductor laser. It should be noted that this device detects the changing phase of a signal without the use of a separate local oscillator as would be the case for conventional homodyne or heterodyne detection. A good choice for the semiconductor laser is a VCSEL and used in all the experiments presented in this Chapter. Due to the short cavity length, small changes in injection light frequency correspond to a measurable change in voltage. A simple experimental verification of the voltage change across the VCSEL device versus input frequency detuning is shown in Figure 3.2 (a) and (b).

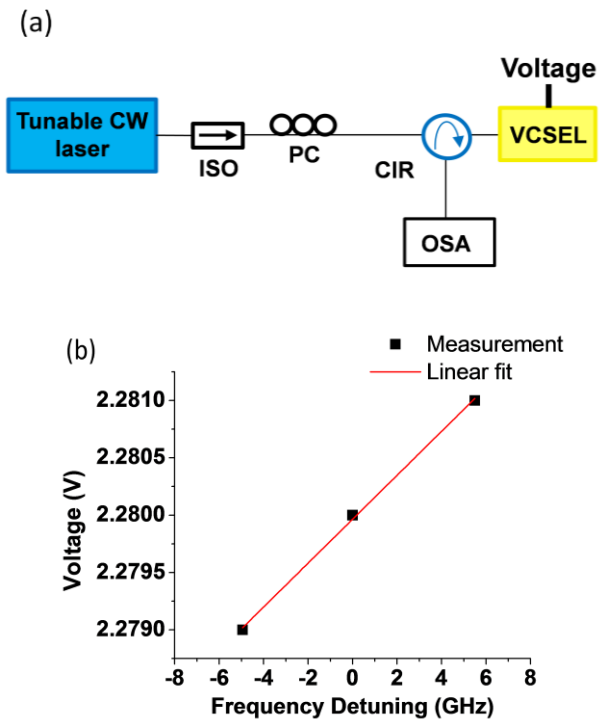

Figure 3.2. Change of the voltage across the active region of injection locked VCSEL (a) schematic of setup (b) Measured voltage vs. frequency detuning.

3.3 Experiments

Two experiments were performed: 1) a single channel experiment demonstrating the direct detection of a phase modulated signal and 2) a multichannel experiment demonstrating simultaneous channel filtering and phase detection. First, the demodulation of the received signal using an injection locked VCSEL in a single channel system is presented.

The schematic of the link implemented with commercially available components is shown in Figure 3.3. A continuous wave (CW) laser operating at 1550 nm with 150

kHz short term (30 sec.) optical frequency stability and narrow linewidth (<1 kHz) is used as the transmitter. The CW light from the laser is sinusoidally phase modulated at an arbitrary frequency (1.702 GHz) using an external lithium niobate phase modulator. It should be noted that the modulation frequency is within the locking range and frequency response of the injection locked VCSEL (-10 dB bandwidth of ~ 5GHz and -3 dB bandwidth of 4.6 GHz). Polarization of the input light to the modulator is adjusted appropriately using the polarization controller placed before the phase modulator to ensure pure phase modulation. The phase modulated light is then sent to a VCSEL after passing through a polarization controller and variable optical attenuator. The latter is used to adjust the amount of injection power. It should be mentioned that the conversion efficiency of this phase detection technique depends on the injection ratio, in addition to the operating bias point of the receiver and the linewidth of the emitter as discussed in [55]. Injection ratio is defined as square root of the ratio of the optical power of the received signal (P_m) to the steady-state power of injection-locked VCSEL (P_s). According to the equation for the half locking range $\Delta\omega_L = f_d\sqrt{1+\alpha^2}\sqrt{\frac{P_m}{P_s}}$, the lower the injection ratio, the smaller the locking range and as a result the VCSEL can be driven across the locking range by the received phase modulated signal. Therefore, the conversion efficiency of the detector is higher for smaller injection ratios. Note f_d is the longitudinal mode spacing and α is the linewidth enhancement factor of the VCSEL.

An optical circulator is placed before the VCSEL to monitor the injection locking process on a high resolution optical spectrum analyzer (OSA). The VCSEL used in this

experiment is a commercially available single mode fiber-coupled device operating at ~1550 nm with side mode suppression of ~51 dB. A bias tee is used to separate the RF and DC components of the voltage across the VCSEL.

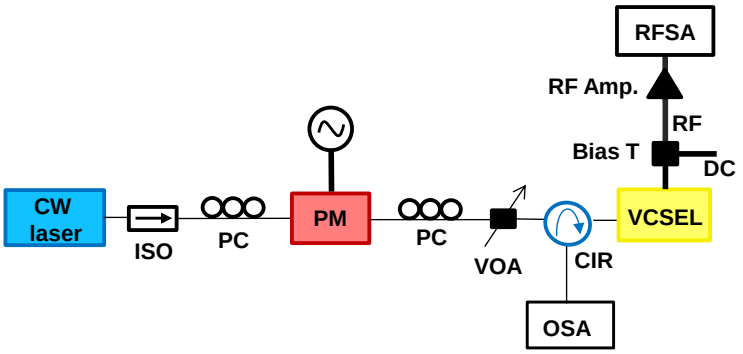

Figure 3.3. Schematic of a single channel system with injection locked VCSEL as the receiver. ISO: isolator, PC: polarization controller, PM: phase modulator, VOA: variable optical attenuator, CIR: circulator, OSA: optical spectrum analyzer, RF Amp.: radio frequency amplifier, RFSA: radio frequency spectrum analyzer.

The RF power spectrum of the converted phase to voltage modulation can be obtained on a RF spectrum analyzer (RFSA). The optical and RF power spectra in two cases are shown in Figure 3.4, when the phase modulated signal is injected to the VCSEL but outside the locking range (Figure 3.4 (a) and (b)) and when the VCSEL is injection locked to the received phase modulated signal (Figure 3.4 (c) and (d)). No RF signal is detected when the VCSEL is not injection locked to the phase modulated signal. However, when the VCSEL is locked to the received signal, an RF tone at frequency of

1.702 GHz is detected. The SNR of the detected signal after proper amplification is ~75 dB/Hz. It should be noted here that the choice of this frequency was completely arbitrary.

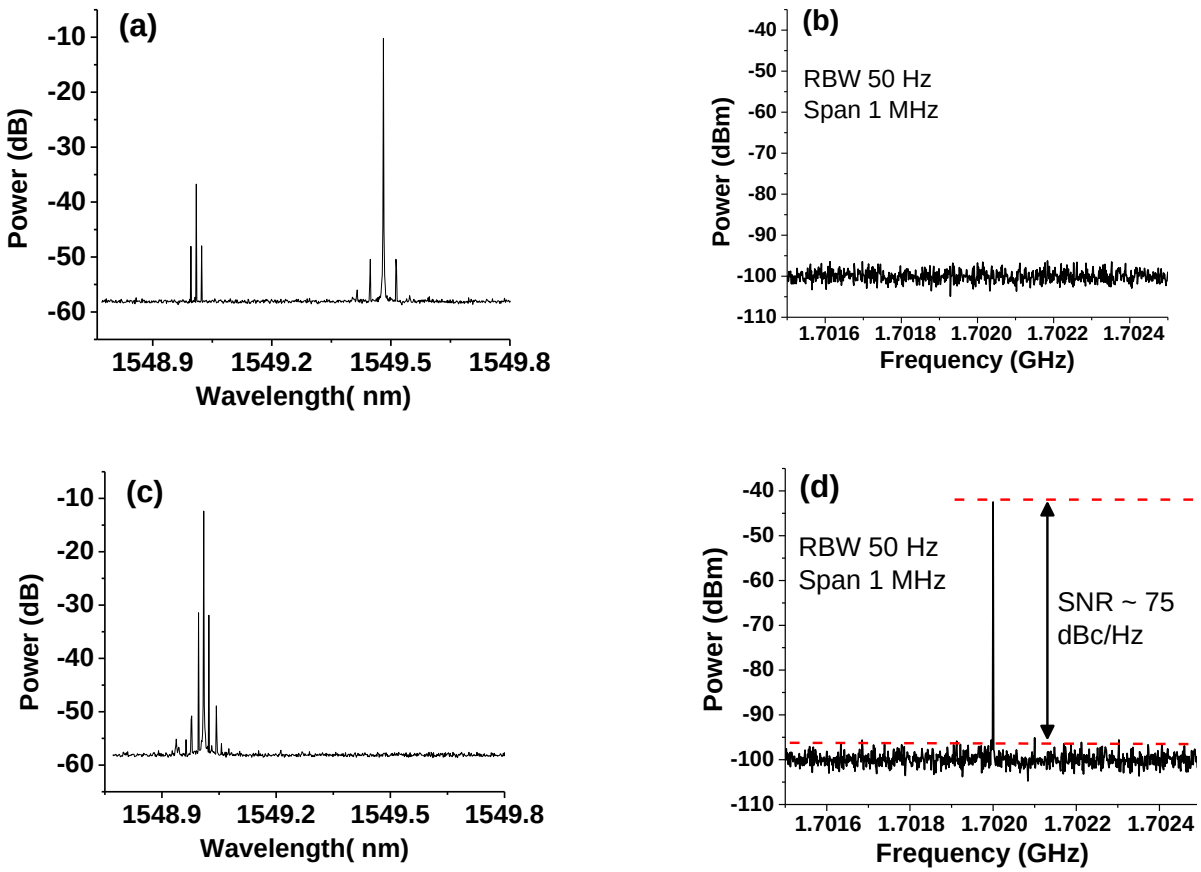

Figure 3.4. Measured optical and RF power spectra. (a)-(b) the phase modulated signal is injected to the VCSEL but outside the locking range.(c)-(d) the VCSEL is locked to the phase modulated signal.

Detected phase modulated signal is also observed on a real-time oscilloscope (60

MHz bandwidth). In this case the phase modulator is sinusoidally modulated at 200 kHz with 4V peak-to-peak amplitude. Detected phase modulated signal and the drive signal of the phase modulator are shown in Figure 3.5.

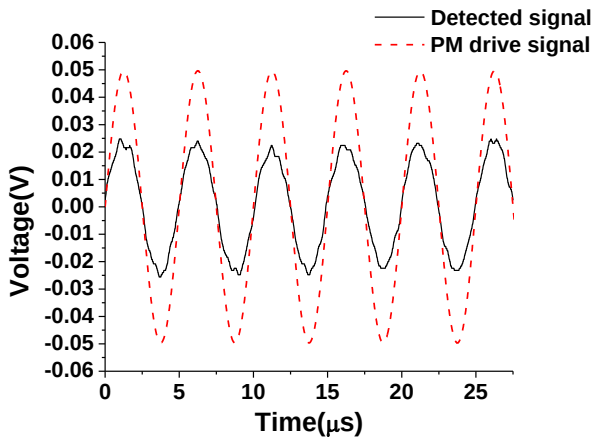

Figure 3.5. Real-time oscilloscope traces of the detected phase modulated signal (solid line) and the drive signal of the phase modulator (dash line). Note that the drive signal is scaled down for better comparison.

In order to demonstrate the channel filtering capabilities of this receiver, a three-channel system was set up, as shown in Figure 3.6. The output of a CW source (~1538.5 nm) is sent to an external lithium niobate intensity modulator (IM) to create side bands separated by 12.5 GHz from the carrier with equal power. A wavelength division multiplexing (WDM) filter with a channel spacing of 6.25 GHz is used to separate the individual optical frequencies. Each channel is independently sinusoidaly phase modulated using an external lithium niobate phase modulator (PM). Phase modulation

frequencies of 0.8 GHz, 0.9 GHz and 1 GHz are chosen for channel 1 through 3, respectively. The independently phase modulated channels are combined with N×1 combiner. The combined channels are injected into the cavity of a VCSEL. The VCSEL used in this experiment is a single mode fiber-coupled device that operates at ~1538.5 nm. It should be noted that the wavelength of the received signal should be within the wavelength tuning range of the VCSEL. For the specific VCSEL device used in this experiment, the lasing wavelength can be tuned over 4 nm by changing the DC bias of the VCSEL.

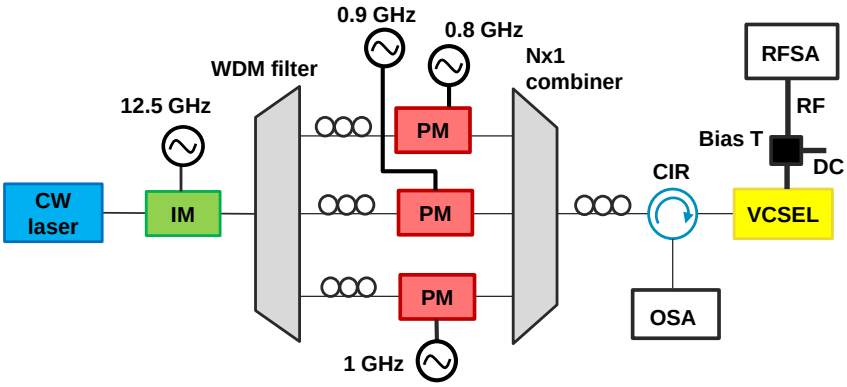

Figure 3.6. Schematic of a three-channel back-to-back link with the injection locked VCSEL as a wavelength selective element and phase detector. IM: Intensity modulator, PM: Phase modulator, CIR: Circulator, VCSEL: Vertical cavity surface emitting laser, OSA: Optical spectrum analyzer, RFSA: Radio frequency spectrum analyzer.

The output optical spectrum of the VCSEL and the injected phase modulated channels when the VCSEL is tuned out of the locking range of these channels is shown in

Figure 3.7, as measured by a high resolution OSA.

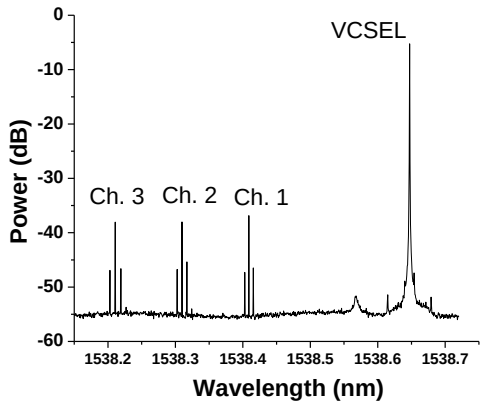

Figure 3.7. Optical spectrum of the VCSEL and the phase modulated signals injected to its cavity. The VCSEL is not locked to any of the channels. Note the phase modulation side bands of the received optical carriers. 0.8 GHz, 0.9 GHz and 1 GHz are the phase modulation frequencies of channels 1 to 3, respectively.

An individual channel can be selected by injection locking the VCSEL to the channel. This can be done by tuning the DC bias of the VCSEL so that the preferred channel will fall within the locking range of the VCSEL. The phase information of the selected channel can be detected by measuring the time-varying voltage across the VCSEL. Figure 3.8(a)-(f) show the optical spectra of the VCSEL injection locked to different channels and the corresponding RF power spectra.

It can be seen that when a channel is selected, for example channel 1(see Figure 3.8 (a)), an RF tone at the phase modulation frequency of the selected optical carrier is observed on the RF power spectrum (see Figure 3.8 (d)). It should be noted that no RF

amplification is performed on the detected RF signal in this case. These results show that the technique described above can be used in multi-channel systems to actively select individual channels as long as the channel spacing is larger than the locking range of the VCSEL.

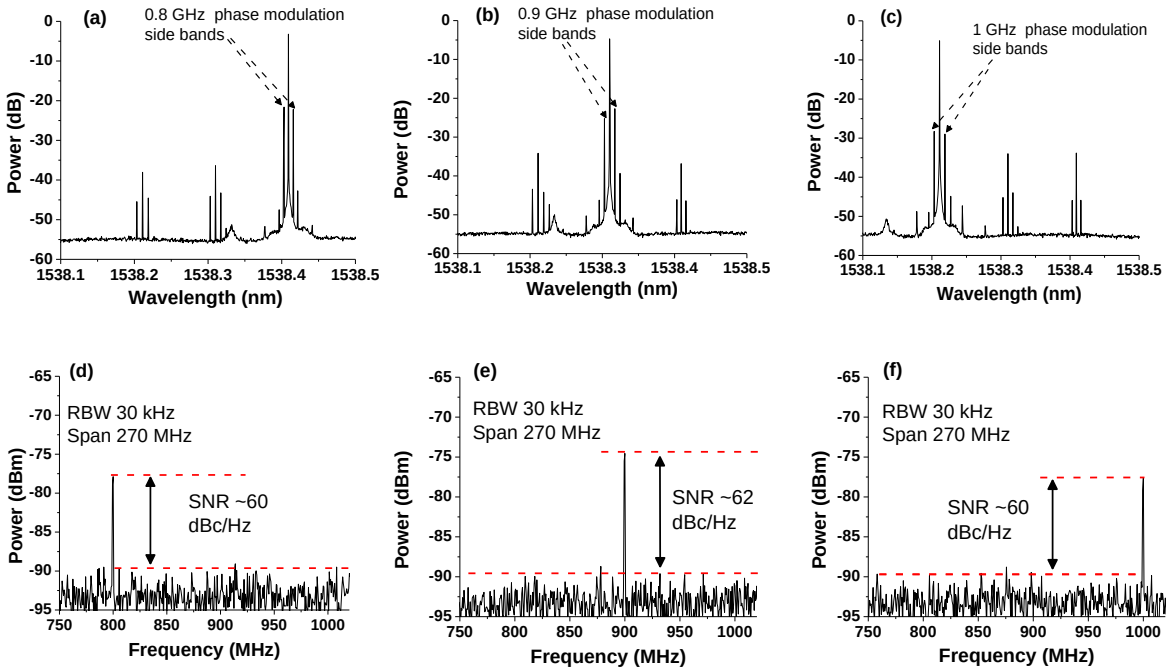

Figure 3.8. Optical spectra (a)-(c) and RF power spectra (d)-(f) of the detected AC voltage across the VCSEL when the VCSEL is injection locked to channels 1 to 3, respectively.

3.4 Application in a cross connect switch

One possible application that can take advantage of the phase modulation and detection properties of an injection locked semiconductor laser is a reconfigurable cross

connect switch. A diagram of such a system is shown in Figure 3.9. From left to right, the input signal is divided and sent to N phase detector (here N=4). Each phase detector is biased to detect the signal on a specific wavelength of the input light. From right to left, the short laser pulse is sent to a WDM filter that separates different colors of light into N channel. Each channel inputs a linear modulator which is biased properly to be able to lock to the input light. The detected electrical signals from the phase detectors are then used to modulate the current of the modulators. The output of the modulators are then recombined in the WDM and sent to the output. Using this method, information from any wavelength can be arbitrary switched between channels and can be done at rates approaching channel spacing.

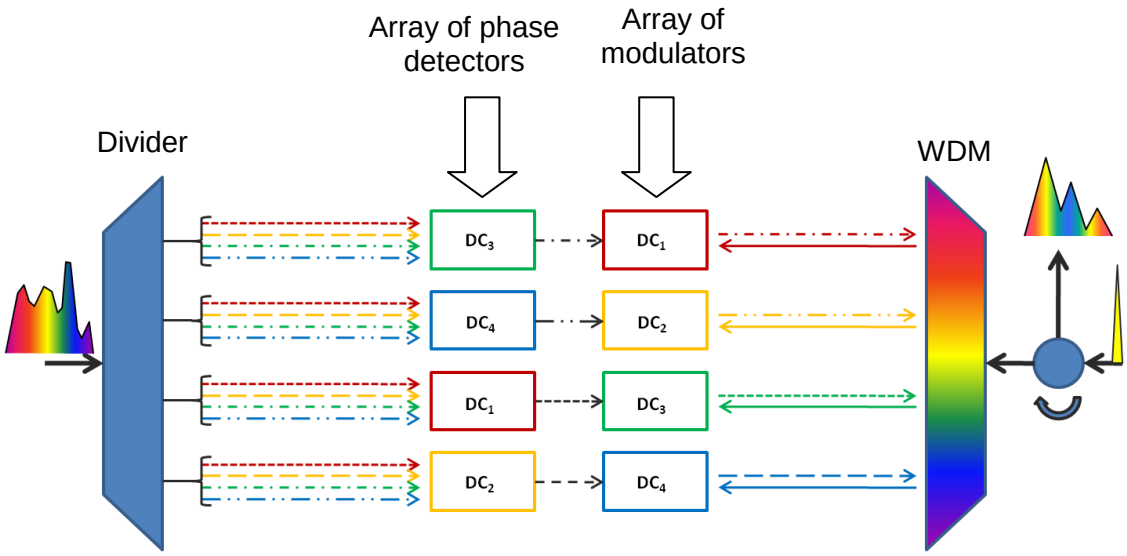

Figure 3.9. Reconfigurable cross connect switch /pulse shaping code reconfiguration using an array of linear modulator and phase detectors.

3.5 Conclusion

A method for detection of phase modulated optical signals using an injection locked VCSEL is experimentally demonstrated. The injection locked VCSEL converts the phase modulation on the optical carrier to a voltage signal across the VCSEL. Using this technique, a sinusoidally phase modulated signal was detected with an SNR of 75dBc/Hz. In a multi-channel system, this method is capable of actively selecting one channel and demodulating its phase information. The process of selecting a channel is achieved by tuning the DC bias of the VCSEL so that the selected channel falls within the locking range of the VCSEL. The experimental results of the performance of the phase detector in a three-channel system are presented. The simplicity of this phase detection technique in addition to channel selection property make this method suitable for detecting phase modulated optical signals in dense WDM systems.

CHAPTER 4: PHASE NOISE OF AN INJECTION LOCKED SEMICONDUCOTR LASER

Experimental measurements of the heterodyne beat between a free running VCSEL and a stable CW source in Figure 2.37 clearly shows the frequency fluctuations of the free running VCSEL. This frequency fluctuation which is within the locking range of the injection-locked VCSEL is converted to phase noise after injection locking. In this Chapter, the phase noise added by an injection-locked semiconductor slave laser is experimentally investigated. It will be shown how the injection ratio and frequency detuning affect the phase noise added by an injection-locked semiconductor laser. The semiconductor slave laser used in all the measurements is a VCSEL and is injection-locked to a narrow linewidth CW fiber laser. This study can help understanding the contribution of the added phase noise by an injection-locked VCSEL to the overall noise floor of the resonant cavity interferometric modulator presented in Chapter 2.

4.1 Self-heterodyne setup

To investigate the phase noise added by an injection-locked semiconductor slave laser (VCSEL) a self-heterodyne beat tone is measured and analyzed. The light from the CW master laser is launched to free space using a fiberized collimator. Using a non-polarizing beam splitter, the light from the master laser is split between the two arms of a Mach-Zehnder interferometer. In one arm of the interferometer, the light from the CW master laser is frequency shifted by 100 MHz using an acousto-optic modulator (AOM). In the other arm of the interferometer, a VCSEL is injection locked to the master laser in

the reflection mode. Polarization of the injection seed is matched with the one from the using VCSEL a polarizer. The injection ratio is controlled by changing the polarization of light before the polarizer. The light from the injection locked VCSEL and frequency shifted master are combined in a non-polarizing beam splitter and coupled into a single mode fiber using a free space coupler. A schematic of the setup is shown in Figure 4.1 .

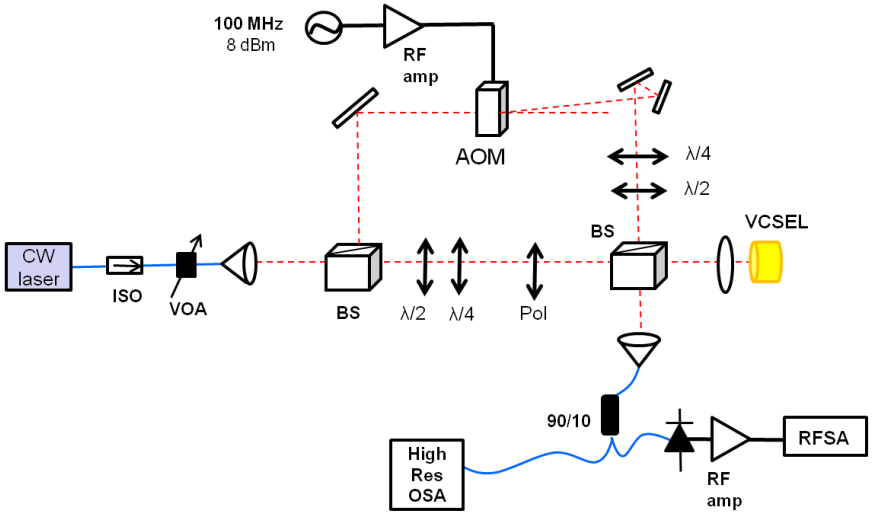

Figure 4.1. A self-heterodyne setup for measuring the phase noise added by an injection locked VCSEL. Iso: Isolator, BS: Beam splitter, AOM: Acousto-optic modulator, Pol: Polarizer, VCSEL: Vertical cavity surface emitting laser, RF. amp: Radio frequency amplifier, RFSA: Radio-frequency spectrum analyzer, High Res OSA: High resolution optical spectrum analyzer.

The collected light is then split using a fiberzied coupler. 90% of the collected light is photodetected and then amplified with a RF amplifier. The 100 MHz beat tone is observed on a RFSA. The other 10% of the light is sent to a high resolution optical spectrum analyzer to monitor the injection locking.

The VCSEL used in this experiment is a free space single mode device at ~1540 nm. Specially designed copper cap is used both as heat sink and a holder for this device. The glass cover on the packaging of the device has been removed to eliminate the reflection. The full beam divergence angle is measured to be 13.2^{o}.

The CW master laser used in these experiments is a narrow linewidth fiber laser (<2 kHz) and center wavelength at 1540 nm. The wavelength of the laser can be tuned by ~ 2 nm by tuning the temperature.

In the first sets of experiments, the injection power was varied from the lowest possible injection power to 4 times more injection power while the VCSEL was kept at a fixed driving current. The self-heterodyne beat tone was measured at each injection ratio. To make the measurements comparable, the optical power on the photodetector was adjusted to be the same for all the measurements. Injection powers reported here are measured right in front of the VCSEL. Only a fraction of this light couples into the cavity due to the front facet reflection and imperfect beam matching between the injection seed beam waist and the VCSEL etc. The results of these measurements for a measurement span of 50 kHz are shown inFigure 4.2. All the measurements were taken with the same resolution bandwidth on the RFSA.

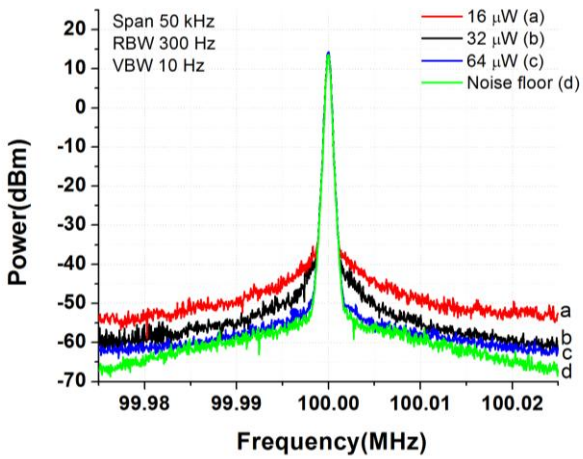

Figure 4.2. Self-heterodyne beat tone at different injection powers.

The noise floor of the measurement was measured by placing a mirror in front of the VCSEL as it is shown in Figure 4.3. Again, the optical power on the photodetector is matched with the previous measurements (with injection locked VCSEL). In Figure 4.2, the green trace (or d) shows the noise floor of the measurement. It can be clearly seen that the phase noise added by the injection locked VCSEL is inversely proportional to the injection ratios.

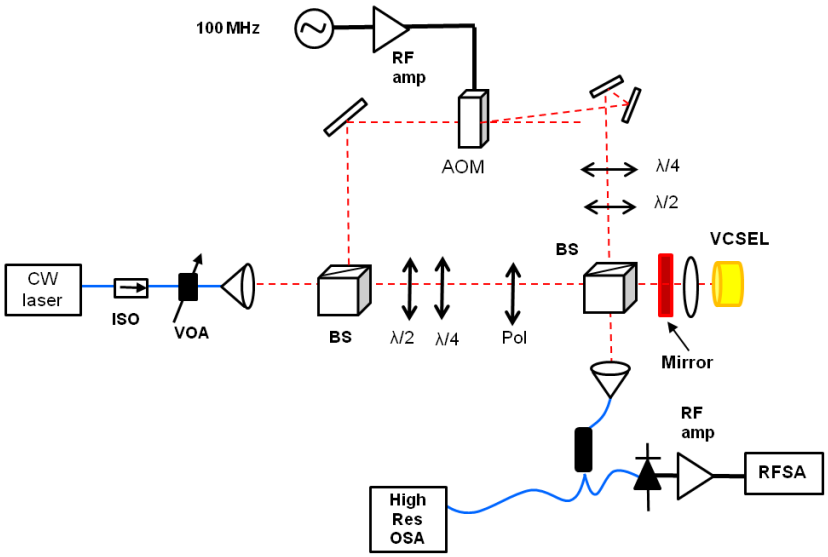

Figure 4.3. Experimental measurement setup for establishing the measurement noise floor. Iso: Isolator, BS: Beam splitter, AOM: Acousto-optic modulator, Pol: Polarizer, VCSEL: Vertical cavity surface emitting laser, RF. amp: Radio frequency amplifier, RFSA: Radio-frequency spectrum analyzer, High Res OSA: High resolution optical spectrum analyzer.

The same measurement was performed with a larger measurement span of 1 MHz of the RFSA and the results are shown in Figure 4.4. The peaks at 200 kHz from the beat tone are due to the master laser relaxation oscillation. The master laser is a fiber laser with known relaxation oscillation tones at 200 kHz. It is interesting to note that the injection locked VCSEL attenuates the master laser relaxation oscillation peaks. The attenuation increases at higher injection powers.

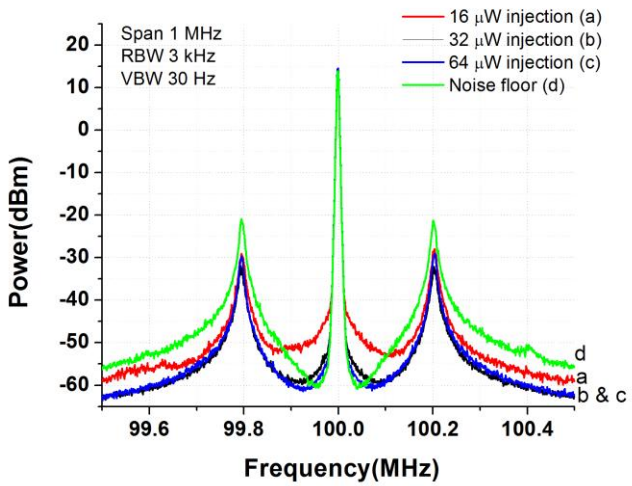

Figure 4.4. Self-heterodyne beat tone at different injection powers. Master laser relaxation oscillation peaks can be seen at 200 kHz offsets from the 100 MHz beat tone.

Next, the effect of frequency detuning of the VCSEL from the master laser frequency on the phase noise added by an injection-locked VCSEL is studied. In this case, the injection power was constant and the detuning frequency was changed by changing the driving current of the VCSEL. Decreasing the DC current of the VCSEL results in an increase of the frequency detuning. The driving current of the VCSEL was varied from 6.87 to 6.84 mA resulting in an increase of the frequency detuning. Optical power on the photodetector is the same in all the measurements. Higher side bands of the beat tone were observed for higher frequency detuning. The results are shown in Figure 4.5.

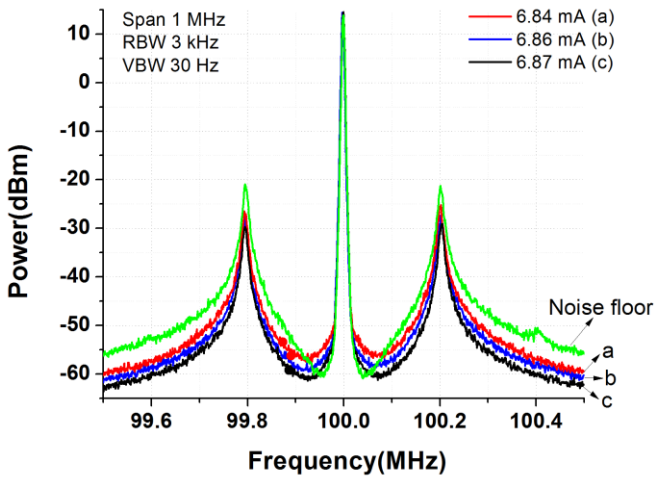

Figure 4.5. Self-heterodyne beat tone at different frequency detuning. Master laser relaxation oscillation peaks can be seen at 200 kHz offsets from the 100 MHz beat tone.

4.2 Conclusion

In this Chapter, the effects of injection power and frequency detuning on the phase noise added by an injection-locked VCSEL are studied. The measurements were done using a self-heterodyn technique. The results show lower added phase noise for higher injection powers. Also, it is shown that the smaller the frequency detuning, the lower the added phase noise of the injection-locked VCSEL.

Interestingly, comparing the noise floor to an injection-locked case in both Figure 4.4 and Figure 4.5, shows attenuation of the power of the master laser relaxation oscillation peaks on the photodetected RF spectrum of the 100 MHz self-heterodyne beat tone. This can be explained by the amplitude response of an injection-locked laser. As it

is mentioned previously, the output power of an injection-locked laser is clamped. Even for injection-locked semiconductor lasers with a non-zero linewidth enhancement factor, the change of the output power is very small. This is the reason for the attenuation of the relaxation oscillation peaks of the master laser after injection locking the slave laser. Higher injection power and smaller frequency detuning result in larger attenuation of the master laser relaxation oscillation peaks by the injection-locked VCSEL.

In conclusion, the phase noise added by the injection-locked VCSEL contributes to the overall noise floor of the system at lower offset frequencies.

CHAPTER 5: FUTURE WORK

In this Chapter, the future directions for the novel resonant cavity linear interferometric intensity modulator proposed and demonstrated in this dissertation are presented. This modulator is the start of a new family of linear modulators and could have a great impact on next generation optical OFDM networks and on-chip integrated optical circuits. The capability of monolithic integration of this modulator with III-V semiconductor devices in addition to its linearity (12 orders of magnitude signal to intermodulation ratio), very low V_π (in the order of 1 mV) and potential overall gain (negative insertion loss), make this modulator a good alternative to the existing EAM technology. A design for integrating the linear interferometric intensity modulator on a monolithic semiconductor chip for CW input light is shown. Also discussed here is the realization of the linear modulator for pulsed light, in which a multi-mode Fabry-Perot laser is used as the resonant cavity.

5.1 Monolithic integration of the linear modulator

So far the novel linear modulator introduced in Chapter 2 has been implemented using fiberized and free space components. This approach has the disadvantages that the modulator's implementation is bulky and the fiber delays drift with environmental changes. The next step for this project, which addresses some of these problems, is to fabricate this modulator on a semiconductor chip. The proposed design for this modulator is shown in Figure 5.1.

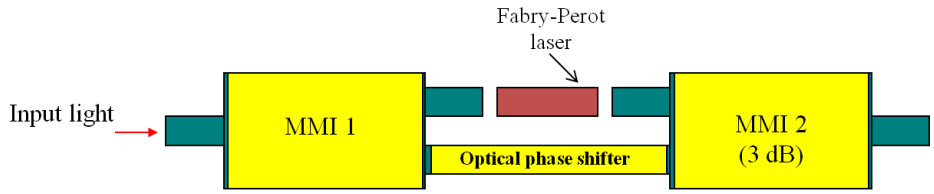

Figure 5.1. Proposed design for the integration of the linear modulator for CW light.

The two multi-mode interference (MMI) sections work as the input and output couplers. In one arm of the interferometer, a simple Fabry-Perot laser is placed. The semiconductor bandgap should be shifted at the MMI and phase control sections to prevent unwanted gain/loss in those sections. This can be achieved using the process of intermixing. In order to realize optical gain, the input MMI section can be designed so that only a small fraction of the input light is used for injection locking the Fabry-Perot laser. The theoretical model provided in Chapter 2 can be used to find the optimum split ratio which corresponds to the weak injection operation regime for a specific device.

As discussed in Chapter 2, the linearity of the modulator response is highly dependent on the operating bias point of the modulator. Thus, an optical phase shifter is considered in the reference arm of the proposed design of the integrated modulator, as it can be seen in Figure 5.1.

5.2 Resonant cavity linear interferometric modulator for pulsed light

In Chapter 2 of this dissertation, a linear resonant cavity interferometric modulator was introduced. This modulator is developed for a CW input light which is

attractive for application in microwave photonics and fiber optic communication systems. Several other optical systems with input pulsed light such as photonic analog to digital converters can benefit from a linear response of such a linear modulator. To adapt this modulation technique for pulsed light, the resonant cavity of the modulator should have multiple resonances within the gain bandwidth. Each mode of the cavity is then injection locks to the closest mode of the input light. By modulating the detuning frequency, each comb line is phase modulated in an arcsine phase fashion. By interfering the modulated signal with its unmodulated counterpart, linear intensity modulation is realized for pulsed light. Figure 5.2 shows the concept of the linear modulator for a pulsed light input.

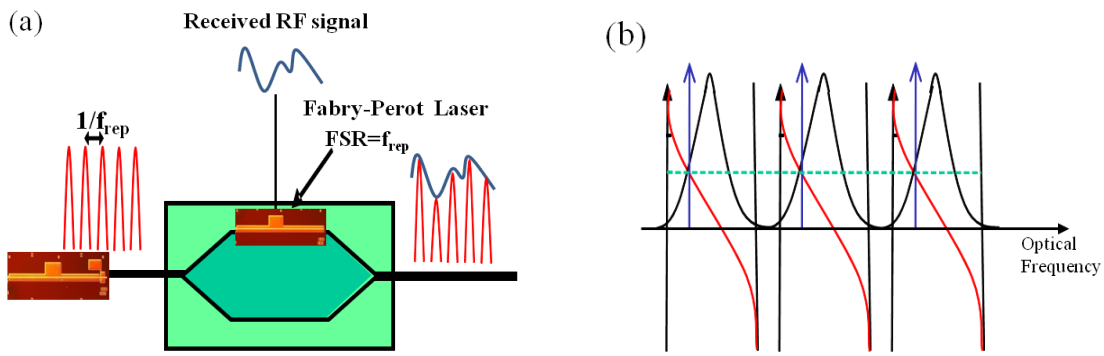

Figure 5.2. (a) A schematic of the linear modulator for pulsed light. (b) The concept of multi-mode injection-locking. Fabry-Perot resonances (in black), the corresponding phase response (in red) and the injected comb lines from the mode locked laser (in blue).

A multi-mode Fabry-Perot laser should be fabricated whose free spectral range (FSR) matches the input pulse repetition rate. This can be a challenging task and careful device fabrication is required to achieve injection locking of all the Fabry-Perot modes to the input pulsed light.

REFERENCES

[1] J. K. A. Pikovsky, M. Rosenblum, *Synchronization: A Universal Concept in Nonlinear Science*. Cambridge University Press, 2001.

[2] R. Adler, "A study of locking phenomena in oscillators," *Proceedings of the IEEE*, vol. 61, no. 10, 1973.

[3] Siegman, "Laser injection locking," in *Lasers*, 1986, pp. 1129-1171.

[4] R. Lang, "Injection locking properties of a semiconductor laser," *IEEE Journal of Quantum Electronics*, vol. 18, no. 6, pp. 976-983, Jun. 1982.

[5] P. Gallion, H. Nakajima, G. Debarge, and C. Chabran, "Contribution of spontaneous emission to the linewidth of an injection-locked semiconductor laser," *IEEE Electronics Letters*, vol. 21, no. 14, pp. 626-628, 1985.

[6] N. A. Olsson et al., "Chirp-free transmission over 82.5 km of single mode fibers at 2 Gbit/s with injection locked DFB semiconductor lasers," *IEEE Journal of Lightwave Technology*, vol. LT–3, no. 1, pp. 63-67, 1985.

[7] Y. Yamamato and T. Kimura, "Coherent optical fiber transmission systems," *IEEE Journal of Quantum Electronics*, vol. QE–17, no. 6, pp. 919-934, 1981.

[8] F. Quinlan, S. Gee, S. Ozharar, and P. Delfyett, "Supermode noise suppression of a harmonically modelocked laser by external optical injection," *Aerospace*, vol. 6243, pp. 1-5, 2006.

[9] S. Piazzolla, P. Spano, and M. Tamburrini, "Small signal analysis of frequency chirping in injection-locked semiconductor lasers," *IEEE Journal of Quantum Electronics*, vol. 22, no. 12, pp. 2219-2223, Dec. 1986.

[10] S. Mohrdiek, H. Burkhard, and H. Walter, "Chirp reduction of directly modulated semiconductor lasers at 10 Gb/s by strong CW light injection," *IEEE Journal of Lightwave Technology*, vol. 12, no. 3, pp. 418-424, Mar. 1994.

[11] X. J. Meng, T. Chau, and M. C. Wu, "Experimental demonstration of modulation bandwidth enhancement in distributed feedback lasers with external light injection," *IEEE Electronics Letters*, vol. 34, no. 21, pp. 2031-2032, Mar. 1998.

[12] X. J. Meng, T. Chau, and M. C. Wu, "Improved intrinsic dynamic distortions in directly modulated semiconductor lasers by optical injection locking," *IEEE Transactions on Microwave Theory and Techniques*, vol. 47, no. 7, pp. 1172-1176, Jul. 1999.

[13] J. Armstrong, “OFDM for Optical Communications,” *IEEE Journal of Lightwave Technology*, vol. 27, no. 3, pp. 189-204, Feb. 2009.

[14] B. Zhang, J. B. Khurgin, and P. a. Morton, “Linearized ring-assisted electrooptical modulator for coherent optical OFDM links,” *IEEE Photonics Technology Letters*, vol. 21, no. 21, pp. 1621-1623, Nov. 2009.

[15] B. E. . Saleh and M. . Teich, *Fundamental of photonics*. Wiley-Interscience, 1991.

[16] P. Yeh and A. Yariv, *Photonics*. Oxford University Press, 2005.

[17] E. K. Lau, X. Zhao, H.-kee Sung, D. Parekh, C. C.- Hasnain, and M. C. Wu, “Strong optical injection-locked semiconductor lasers demonstrating > 100-GHz resonance frequencies and 80-GHz intrinsic bandwidths,” *Optics Express*, vol. 16, no. 9, pp. 6609-6618, 2008.

[18] G. P. Agrawal, *Fiber-optic communication systems*. 1997.

[19] A. Yariv, *Optical electronics in modern communications*. 1996.

[20] C. H. Cox, E. I. Ackerman, G. E. Betts, and J. L. Prince, “Limits on the performance of RF-over-fiber links and their impact on device design,” *IEEE Transactions on Microwave Theory and Techniques*, vol. 54, no. 2, pp. 906-920, 2006.

[21] K. Noguchi, O. Mitomi, and H. Miyazawa, “Millimeter-Wave Ti:LiNbO3 Optical Modulators,” *IEEE Journal of Lightwave Technology*, vol. 16, no. 4, pp. 615-619, Apr. 1998.

[22] G. E. Betts, L. M. Johnson, and C. H. Cox, “High-sensitivity lumped-element bandpass modulators in LiNbO3,” *IEEE Journal of Lightwave Technology*, vol. 7, no. 12, pp. 2078-2083, 1989.

[23] J. D. Mckinney, K. Colladay, and K. J. Williams, “Linearization of phase-modulated analog optical links employing interferometric demodulation,” *IEEE Journal of Lightwave Technology*, vol. 27, no. 9, pp. 1212-1220, 2009.

[24] T. Ishibashi, N. Shimizu, S. Kodama, H. Ito, T. Nagatsuma, and T. Furuta, “Uni-traveling-carrier photodiodes,” in *Ultrafast Electronic and Optoelectronics*, 1997, vol. 13, pp. 83-86.

[25] R. G. Walker, “High-speed III-V semiconductor intensity modulators,” *IEEE Journal of Quantum Electronics*, vol. 27, no. 3, pp. 654-667, Mar. 1991.

[26] R. Spickermann, S. R. Sakamoto, M. G. Peters, and N. Dagli, “GaAs/AlGaAs travelling wave electro-optic modulator with an electrical bandwidth >40 GHz,” *IEEE Electronics Letters*, vol. 32, no. 12, pp. 1095-1096, 1996.

[27] D. Chen et al., “Demonstration of 110 GHz electro-optic polymer modulators,” *Applied Physics Letters*, vol. 70, no. 25, pp. 3335-3337, 1997.

[28] B. Liu, J. Shim, A. Chiu, A. Keating, J. Piprek, and J. Bowers, “Analog characterization of low-voltage MQW traveling-wave electro absorption modulators,” *IEEE Journal of Lightwave Technology*, vol. 21, pp. 3011-3019, 2003.

[29] Y.-jen Chiu, Chou.H, V. Kaman, P. Abraham, and J. Bowers, “High extinction ratio and saturation power traveling-wave electro-absorption modulator,” *IEEE Photonics Technology Letters*, vol. 14, pp. 792-794, 2002.

[30] B. B. Dingel, “Ultra-linear, broadband optical modulator for high performance analog fiber link system,” in *IEEE International Topical Meeting on Microwave Photonics*, 2004, pp. 241-244.

[31] X. Xie, J. Khurgin, J. Kang, and F.-san Chow, “Linearized Mach–Zehnder intensity modulator,” *IEEE Photonics Technology Letters*, vol. 15, no. 4, pp. 531-533, 2003.

[32] A. Djupsjobacka, “A linearization concept for integrated-optic modulators,” *IEEE Photonics Technology Letters*, vol. 4, no. 8, pp. 869-872, 1992.

[33] G. E. Betts, “A linearized modulator for high performance bandpass optical analog links,” in *IEEE MTT-S Digest*, 1994, pp. 1097-110.

[34] C. H. Cox, *Analog Optical Links: Theory and Practice*. Cambridge Studies in Modern Optics, 2004.

[35] R. Sadhwani and B. Jalali, “Adaptive CMOS predistortion linearizer for fiber-optic links,” *IEEE Journal of Lightwave Technology*, vol. 21, no. 12, pp. 3180-3193, 2003.

[36] G. C. Wilson et al., “Predistortion of electroabsorption modulators for analog CATV systems at 1.55 μm,” *IEEE Journal of Lightwave Technology*, vol. 15, no. 9, pp. 1654-1662, 1997.

[37] R. Vahldieck and D. Hassin, “Feedforward linearization of analog modulated laser diodes-theoretical analysis and experimental verification,” *IEEE Transactions Microwave Theory Techniques*, vol. 41, no. 12, pp. 2376 - 2382, 1993.

[38] D. Novak, “Enabling microwave photonic technologies for antenna remoting,” *IEEE LEOS Newsletter*, vol. 23, pp. 21-24, 2009.

[39] J. B. Khurgin and P. a. Morton, “Linearized ring-assisted electrooptical modulator for coherent optical OFDM links,” *IEEE Photonics Technology Letters*, vol. 21, no. 21, pp. 1621-1623, Nov. 2009.

[40] S. Li, X. Zheng, H. Zhang, and B. Zhou, “Highly linear radio-over-fiber system incorporating a single-drive dual-parallel Mach – Zehnder modulator,” *IEEE Photonics Technology Letters*, vol. 22, no. 24, pp. 1775-1777, 2010.

[41] G. Zhu, W. Liu, and H. R. Fetterman, “A broadband linearized coherent analog fiber-optic link employing dual parallel Mach – Zehnder modulators,” *IEEE Photonics Technology Letters*, vol. 21, no. 21, pp. 1627-1629, 2009.

[42] U. Cummings, “Linearized and high frequency electro-optic modulators,” California Institute of Technology, Pasadena, California, 2005.

[43] J. H. Schaffner et al., “Spur-free dynamic range measurements of fiber optic link with traveling wave linearized directional coupler modulators,” *IEEE Photonics Journal*, vol. 6, no. 2, pp. 6-8, 1994.

[44] D. J. F. Barros and J. M. Kahn, “Optical modulator optimization for orthogonal frequency-division multiplexing,” *IEEE Journal of Lightwave Technology*, vol. 27, no. 13, pp. 2370-2378, 2009.

[45] N. Hoghooghi, I. Ozdur, M. Akbulut, J. Davila-rodriguez, and P. J. Delfyett, “Resonant cavity linear interferometric intensity modulator,” *Optics Letters*, vol. 35, no. 8, pp. 1218-1220, 2010.

[46] S. Kobayashi and T. Kimura, “Optical phase modulation in an injection locked AlGaAs semiconductor laser,” *IEEE Transactions on Microwave Theory and Techniques*, vol. MTT–30, no. 10, pp. 1650-1657, 1982.

[47] F. Mogensen, H. Olesen, and G. Jacobsen, “Locking conditions and stability properties for a semiconductor laser with external light injection,” *IEEE Journal of Quantum Electronic*, vol. QE–21, no. 7, pp. 784-793, 1985.

[48] E. K. Lau, L. J. Wong, and M. C. Wu, “Enhanced modulation characteristics of optical injection-locked lasers : A tutorial,” *IEEE Journal of Selected Topics in Quantum Electronics*, vol. 15, no. 3, pp. 618-633, 2009.

[49] C. H. Chang, L. Chrostowski, and C. J. Chang-hasnain, “Injection locking of VCSELs,” *IEEE Journal of Selected Topics in Quantum Electronics*, vol. 9, no. 5, pp. 1386-1393, 2003.

[50] H. Li, T. L. Lucas, J. G. McInerney, M. W. Wright, and R. A. Morgan, “Injection locking dynamics of vertical cavity semiconductor lasers under conventional and phase conjugate injection,” *IEEE Journal of Quantum Electronics*, vol. 32, no. 2, pp. 227-235, 1996.

[51] N. Hoghooghi and P. J. Delfyett, “Theoretical and experimental study of a semiconductor sesonant cavity linear interferometric intensity modulator,” *IEEE Journal of Lightwave Technology*, vol. 29, no. 22, pp. 3421-3427, 2011.

[52] C. H. Henry, N. A. Olsson, and N. K. Dutta, “Locking range and stability of injection locked 1.54 μm InGaAsP semiconductor lasers,” *IEEE Journal of Quantum Electronics*, vol. QE–21, no. 8, pp. 1152-1156, 1985.

[53] S. Yamashita and T. Okoshi, “Suppression of common-mode beat noise from optical amplifiers using a balanced receiver,” *Electronics Letters*, vol. 28, no. 21, pp. 1970-1972, 1992.

[54] R. Helkey, “Relative-intensity-noise cancellation in bandpass external-modulation links,” *IEEE Transactions on Microwave Theory and Techniques*, vol. 46, no. 12, pp. 2083-2091, 1998.

[55] O. Lidoyn and P. Gallion, “Analysis of receiver using injection locked semiconductor laser for direct demodulation of PSK optical signals,” *IEEE Electronics Letters*, vol. 27, no. 11, pp. 995-997, 1991.

[56] L. a. Johansson and L. a. Coldren, “Wavelength-tunable receiver channel selection and filtering using SG-DBR laser injection-locking,” in *Optical Fiber Communication Conference*, 2005.

[57] G. H. . Thompson, “Appendix 4,” in *Physics of semicondcutor lasers devices*, Wiley, 1988.